

Quantitative Morphological Analysis of the HDF North and HDF-South. I. Early{} and Late{} type Lum inosity{} Size Relations of galaxies out to $z = 1$

I. Trujillo^{1?} and J.A.L.Aguerri^{2?}

¹Max-Planck-Institut für Astronomie, Königstuhl 17, D-69117 Heidelberg, Germany

²Instituto de Astrofísica de Canarias, Calle Vía Láctea, E-38200 La Laguna, Tenerife, Spain

Accepted 0000 December 00. Received 0000 December 00; in original form 0000 October 00

ABSTRACT

Based on drizzled F606W and F814W images, we present quantitative structural parameters in the V-band rest-frame for all galaxies with $z < 1$ and $I_{814}(\text{AB}) < 24.5$ mag in the Hubble Deep Fields North and South. Our structural parameters are based on a two-component surface brightness distribution using a Sersic bulge and an exponential disc. Detailed simulations and comparisons with previous work are presented. The luminosity-size distribution of early-type galaxies is consistent with the hypothesis that their structural properties were already in place by $z = 1$ and have evolved passively since then; early-type galaxies were $1.35(0.1)$ mag brighter in rest-frame V-band luminosity at $z = 0.7$ than now. Compared to present day late-type galaxies, those at $z = 0.7$ with $L_V > 0.2 \cdot 10^{10} h^{-2} L_\odot$ show a moderate decrease ($30(10)\%$) in size (or interpreted directly, a decrease of $0.77(0.30)$ mag in the central surface brightness) at a given luminosity. Finally, we make a comparison of our results with the infall and hierarchical models.

Key words: galaxies: distances and redshift - galaxies: evolution - galaxies: photometry - galaxies: fundamental parameters

1 INTRODUCTION

The Hubble Deep Field (HDF) North (Williams et al. 1996) and South (Casertano et al. 2000) are among the deepest views of the universe ever obtained. These observations were specially made to facilitate the study of galaxy evolution. The high resolution of the publicly available drizzled images ($0.04''/\text{pix}$, i.e. $0.22 h^{-1} \text{kpc}$ at $z = 1$) convert them into an ideal laboratory for morphological evolutionary studies.

Morphology plays a fundamental role in understanding galaxy evolution as each galaxy type could evolve differently with z . To facilitate the comparison with the theoretical predictions, galaxy evolution studies must be rooted in a quantitative basis. In addition, quantitative morphology enables one to study any possible evolution of the galaxy structural parameters such as luminosity, size, etc., and their associated scaling relations with regards to the values measured in nearby samples.

In the hierarchical galaxy formation framework, both disc and elliptical galaxy properties are expected to evolve at high z . In this paradigm, it is generally assumed that much of a galaxy's star formation takes place in a galactic disc which formed by gas infall into dark matter halos (White & Frenk 1991; Kauffmann et al. 1999; Somerville & Primack 1999). According to Mo, Mao & White (1998) the size of the disc galaxies, at a fixed halo circular velocity, must decrease with redshift as $R \propto H(z)^{-1}$ where $H(z)$ is the Hubble parameter at redshift z . On the other hand, E/S0 galaxies are expected to form via repeated merging (Toomre & Toomre 1972). The formation epoch of the E/S0 galaxies is sensitive to the assumed values of cosmological parameters, occurring at higher redshift at lower M (Kauffmann & Charlot 1998).

There are alternative theories of galaxy formation. One is that all galaxies, including E/S0, formed very early via monolithic collapse of the gas at high redshift (Eggen, Lynden-Bell & Sandage 1962; Larson 1975; Chiosi & Carraro 2002). According to this theory E/S0 properties will be already in place at high z . For disc galaxies, some "backward" approaches have been tried. These approaches use the detailed studies of the profiles of the Milky Way and

? Email: trujillo@mpia-hd.mpg.de (IT); jalfonso@iac.es (JALA)

¹ We adopt a cosmology throughout the paper with $M = 0.3$, $\Omega_0 = 0.7$ and $H_0 = 100 h \text{ km s}^{-1} \text{ Mpc}^{-1}$.

2 I. Trujillo and J A L . Aguerri

other nearby galaxies to propose radially dependent models of star formation that could be used to make predictions about high-z disc evolution (Cayon, Silk & Charlot 1996; Bouwens, Cayon & Silk 1997; Roche et al. 1998). However, both the hierarchical and "backward" models predict relatively similar amounts of evolution in disc global properties (size, luminosity, etc.) to $z \approx 1$ (Bouwens & Silk 2002).

The field covered by both HDF's is not large compared to others works but they are so deep that they are significantly less affected by the incompleteness problem affecting other less deep samples. Discrepancies associated to incompleteness can be found in the literature, for example, studying disc galaxies, Schade et al. (1995, 1996) who used early ground- and space-based images of galaxies from the Canada-France Redshift Survey (CFRS) and Roche et al. (1998) in the Medium Deep Survey found a net increase in the surface brightness and a net decrease in the size. However, Simard et al. (1999), who conducted a detailed analysis of the selection effects in the Deep Extragalactic Evolutionary Probe (DEEP) survey found no evolution in disc properties up to $z \approx 1$.

In the following work we conduct a detailed morphological analysis of all the galaxies with $z < 1$ in the HDF (North and South) on the drizzled F 606W and F 814W images down to $I_{814}(\text{AB}) = 24.5$ mag. Quantitative morphological analysis can be conducted using non-model-based techniques like the concentration and asymmetry of the galactic light (Abraham et al. 1996). However, these techniques have the disadvantage that they do not allow the study of the different structural components of the galaxy separately, and particularly, the evolutionary analysis of the well known local scale relation can not be addressed.

Improving upon previous analyses, our structural parameters are based on a two-component surface brightness distribution using a Sersic $r^{1/n}$ bulge (Sersic 1968) and an exponential disc. A previous detailed morphological analysis of the HDF (N) was carried by Marleau & Simard (1998, hereafter M+S98). However, that work only considered a $r^{1/4}$ bulge, instead of a free $r^{1/n}$. Our assumption of a free bulge is more in agreement to what it is observed in the nearby universe (see, e.g. Graham 2001 and references therein). On the other hand, even though the nearly identical quality of the HDF (S), a systematic quantitative morphological analysis of this field have been not yet conducted and it is of great interest to compare the galaxy properties between these two fields.

In this paper we present the galaxy structural parameters of both HDF fields and compare our results to previous classification schemes. To assess the degree of evolution, if any, the early- and late-type luminosity-size relations are compared with those observed in the nearby universe provided by large local surveys such as the Sloan Digital Sky Survey (York et al. 2000). In a second paper (Aguerri & Trujillo 2004), we analyse the redshift evolution of the structural components of the galaxies (bulge and disc) separately. The outline of this paper is as follows: section 2 describes the characteristics of the observed fields. Our quantitative morphological analysis algorithm is explained in section 3. In section 4 we detail our object morphological classification and in section 5 we analyse the accuracy of our analysis by comparing our results with simulations and previous work. Section 6 deals with the issue of selection effects. The

luminosity-size relations of early- and late-type galaxies are presented in section 7. We discuss our results in section 8.

2 DATA

Each HDF image consists on a $2.5' \times 2.5'$ arcmin 2 wide Field Planetary Camera 2 (WFPC2) pointing (Williams et al. 1996, HDF(N); Casertano et al. 2000, HDF(S)). The images were acquired through the broad band F 300W, F 450W, F 606W, and F 814W filters. For the present work we have used the publically available reduced F 606W and F 814W Version 2 drizzled images with a sampling of 0.04 arcsec/pixel and a total exposure time of 109050 s (F 606W HDF(N)), 123600 s (F 814W HDF(N)), 97200 s (F 606W HDF(S)) and 112200 s (F 814W HDF(S)). The high sampling of these images avoids the undersampling problem affecting other Hubble Space Telescope (HST) images.

In order to assure a reliable estimation of the structural parameters (see the simulations section) we have selected all the $I_{814}(\text{AB}) < 24.5$ galaxies with $z < 1$. In addition, to maintain the analysis in the V-band rest-frame, we have also studied the $I_{814}(\text{AB}) < 24.5$ galaxies with $z < 0.4$ in the F 606W filter. The above restrictions leave us with 123 objects in the HDF(N) and 95 in the HDF(S). The redshift and total magnitude information was obtained from two photometric redshift catalogs: Fernandez-Soto, Lanzetta & Yahil, (1999; HDF(N)) and Labbe et al. (2003; HDF(S)). The HDF(N) catalog provides aperture magnitudes which are then corrected for the effect of neighboring. These magnitudes correspond to the SExtractor magnitudes named as "best". For the HDF(S) catalog, Labbe et al. provide with a "color" aperture (see their sec. 5.2). This "color" aperture is an isophotal aperture determined by the K_s -band detection isophote at the 5% detection threshold when the galaxies satisfy a "size" criteria, and is a fixed aperture when the galaxies are outside this "size" range. This "color" magnitude is finally transformed to a total magnitude using the total magnitude in the K_s -band. The total K_s -band magnitude is based on a Kron-like aperture (SE \times AUTO) derived from the K_s -band detection image. When available, spectroscopic redshifts are used. This corresponds to 70% of the galaxies in the HDF(N) and 60% in the HDF(S) in the present work.

The number identifications of the objects correspond to the same numbers used in the photometric redshift catalogs.

3 THE FITTING ALGORITHM

Our morphological analysis is based on the decomposition of the surface brightness (SB) profile into a bulge and a disc component. The bulge component is modeled by a Sersic (1968) profile of the form:

$$I(r) = I_b(0)e^{-b_n(r=r_{e,b})^{1/n}} \quad (1)$$

where $I_b(0)$ is the bulge central intensity, $r_{e,b}$ is the bulge semi-major effective radius and n the Sersic shape parameter. The intensity at the bulge effective radius $r_{e,b}$ is given by $I_{e,b} = I_b(0)e^{-b_n}$. The quantity b_n is a function of the shape parameter n , and is chosen so that $r_{e,b}$ encloses half of the total luminosity. The exact value is derived from $(2n) = 2 - (2n/b_n)$, where (a) and $(a;x)$ are the gamma

and the incomplete gamma function (Abramowitz & Stegun 1964, p.260). The Sersic model contains the classical de Vaucouleurs profile when n is equal to 4. The disc component is an exponential profile (Freeman 1970) given by:

$$I(r) = I_d(0)e^{-r/h} \quad (2)$$

where $I_d(0)$ is the central intensity and h is the disc semi-major scale length. The set of free parameters is completed with the ellipticities of the bulge b and the disc d . In addition, it is possible to determine from the above parameters the total magnitude:

$$I_{814}(\text{mag}) = 2.5 \log(F_b + F_d) + C \quad (3)$$

where t is the exposure time, C is the zeropoint, F_b is the bulge luminosity $F_b = I_b(0)r_{e,b}^2(1-b)^2 n(2n-b)^{2n}$ and F_d is the disc luminosity $F_d = I_d(0)h^2(1-d)^2$. We have used $C = 23.02$ (F606W) and $C = 22.09$ (F814W) in the AB system.

We can also evaluate the bulge-to-total luminosity ratio B/T :

$$\frac{B}{T} = \frac{F_b}{F_b + F_d} \quad (4)$$

and the global semi-major effective radius r_e by solving the equation:

$$\frac{B=T}{1-B=T} = 1 - \frac{2(2n;b_n(r_e=r_{e,b})^{1/n})}{(2n)} = 2(2;r_e=h) - 1 \quad (5)$$

Our parameter recovering method is described in detail in Trujillo et al. (2001a) and Aguerri & Trujillo (2002). The main points of the routine are as follows. The final SB distributions resulting from the convolution between the Point Spread Function (PSF) and our 2D Sersic model SB distribution are dependent on the intrinsic ellipticity of the original source. However, to evaluate the intrinsic ellipticity of a model (i.e. the value of the ellipticity of the isophotes before being affected by the seeing) it is often insufficient to simply measure the ellipticity at one given radial distance. The ellipticity of the isophotes is reduced by seeing and this reduction depends on the radial distance of the isophote to the centre of the model, the size of the seeing, and the values of the model parameters (Trujillo et al. 2001b,c). For that reason, the determination of the intrinsic ellipticity of the source and the fitting process to determine the structural parameters must be done in tandem (i.e. iteratively and self-consistently). To do this we simultaneously fit both the observed 1D SB and ellipticity semi-major axis radial profiles using convolved profiles for each. We illustrate our technique in Fig. 1.

The measured SB and ellipticity semi-major radial profiles are obtained from fitting ellipses to the isophotes of the selected objects. The elliptical isophotes are measured using the task ELLIPSE within IRAF² and fitting down to 1.5 (where σ is the standard deviation of the sky background of the images). A Levenberg-Marquardt non-linear fitting algorithm (Press et al. 1992) was used to determine the set

of free parameters which minimizes χ^2 . A variety of starting parameters are used to ensure that our fits do not get trapped in local χ^2 minima.

The PSF was estimated fitting a Moffat function to star profiles. The high sampling of the drizzled images that we used and the presence of enough non-saturated stars along the field of view facilitates the estimation of the PSF properties by a direct fit to this simple analytical function. We find that a Moffat function with the parameters presented below reproduces the observed PSF very well. We have estimated a 5 per cent uncertainty in the estimation of the FWHM due to changes from one WFPC2 position to another. In addition, the use of an analytical PSF facilitates a robust analytical estimation of the convolution between the PSF and the Sersic profile.

We find the following and FWHM (Full at Width Half Maximum) as our best-fitting stellar parameters: $\beta = 3$, FWHM = $0\farcs142$ (F606W); $\beta = 2.5$, FWHM = $0\farcs147$ (F814W). The best-fitting galaxy parameters in the F814W band are shown in Table 1. There, we list the following:

(1) The galaxy identification number as appearing in the photometric redshift catalogs Fernandez-Soto, Lanzetta & Yahil, (1999; HDF{N) and Labbe et al. (2003; HDF{S).

(2) and (3) Right Ascension and Declination (J2000 coordinates).

(4) Best AB (8140) model-independent magnitudes according to the photometric catalogs.

(5) The surface brightness of the bulge at the effective radius (mag/arcsec² in the I₈₁₄ band).

(6) The semi-major effective radius of the bulge (arcsec).

(7) The Sersic index n of the bulge.

(8) The ellipticity of the bulge.

(9) The central surface brightness of the disc (mag/arcsec² in the I₈₁₄ band).

(10) The semi-major scale length of the disc (arcsec).

(11) The ellipticity of the disc.

(12) The bulge-to-total luminosity ratio ($B=T < 0$ indicates galaxies classified as irregular/peculiar/merger systems).

(13) Spectroscopic redshift unless the index "a" appears which means photometric redshift from Fernandez-Soto, Lanzetta & Yahil, (1999; HDF{N) and Labbe et al. (2003; HDF{S).

(14) Total AB (8140) magnitude as derived from the model fit.

(15) The global semi-major effective radius of the galaxy (arcsec).

For galaxies with $z < 0.4$ the best-fitting galaxy parameters in the F606W band are shown in Table 2.

Our code has already been used and tested in a variety of HST and ground-based studies of nearby and distant galaxies: the quantitative morphological analysis of galaxies in Abell 2443 (Trujillo et al. 2001a) and Coma (Gutierrez et al. 2004; Aguerri et al. 2004) clusters, the number density evolution of galaxies in the SSA 13 and SSA 22 Hawaiian Deep Fields (Aguerri & Trujillo 2002), the ISAAC near-infrared images of the HDF{S (Trujillo et al. 2004) and the F栏king Fields HST images (Graham et al. 2004). In Trujillo et al. (2004) we have also made a comparison between our code and the GALFIT code (Peng et al. 2002) finding an excellent agreement.

² IRAF is distributed by the National Optical Astronomical Observatories, which are operated by AURA, Inc. under contract to the NSF.

Table 1. Best Morphological Parameter Values For Galaxies with I_{814} (AB) < 24.5 mag and $z < 1$ in the HDF{N} and HDF{S}.

(1) ID	(2) R A .(J2000) (h m s)	(3) D .(J2000) (m s)	(4) I_{814} (cat) mag	(5) $r_{e;b}$ mag/ ''^2	(6) $r_{e;b}$ ("	(7) n	(8) b	(9) $d(0)$ mag/ ''^2	(10) d (0) mag/ ''^2	(11) h ("	(12) B /T	(13) z	(14) I_{814} (mod) mag	(15) r_e ("
HDF{N}														
1	12:36:57.47	62:12:10.5	21.2	20.3	0.10	2.91	0.20	20.99	0.36	0.34	0.36	0.665	21.1	0.38
6	12:36:57.45	62:12:11.8	23.2	21.3	0.06	1.09	0.21	22.11	0.24	0.14	0.20	0.561	23.1	0.31
7	12:36:57.60	62:12:12.3	23.1	24.2	0.08	1.38	0.71	22.91	0.36	0.26	0.01	0.920 ^a	23.4	0.59
10	12:36:51.95	62:11:55.3	23.7	23.9	0.12	0.55	0.35	23.45	0.52	0.38	0.05	0.080 ^a	23.3	0.82
11	12:36:56.42	62:12:09.2	23.2	0.00	0.00	0.00	0.00	21.70	0.33	0.61	0.00	0.321	23.1	0.50
12	12:36:44.74	62:11:33.4	24.4	23.5	0.16	2.95	0.11	0.000	0.00	0.00	1.00	0.880 ^a	24.4	0.16
18	12:36:49.24	62:11:48.4	22.9	0.00	0.00	0.00	0.00	20.92	0.21	0.37	0.00	0.961	22.8	0.37
33	12:36:59.37	62:12:21.6	24.0	25.1	0.01	10.6	0.59	22.85	0.31	0.38	0.00	0.472	23.9	0.51
54	12:36:58.65	62:12:21.7	23.3	0.00	0.00	0.00	0.00	20.69	0.14	0.30	0.00	0.681	23.3	0.22
55	12:36:41.97	62:11:30.3	23.3	0.00	0.00	0.00	0.00	23.15	0.55	0.67	0.00	0.200 ^a	23.8	0.69
81	12:36:45.30	62:11:42.8	23.9	23.5	0.53	0.30	0.64	0.000	0.00	0.00	-1.00	0.558	23.7	0.53
85	12:36:41.61	62:11:31.8	19.7	21.8	0.34	0.46	0.40	20.72	0.81	0.70	0.14	0.089	20.3	1.15
91	12:36:42.28	62:11:34.7	23.8	22.8	0.15	0.27	0.64	23.26	0.34	0.26	0.14	0.760 ^a	23.7	0.48
122	12:36:43.80	62:11:42.8	20.8	23.6	0.91	6.32	0.25	0.000	0.00	0.00	1.00	0.764	20.4	0.91
124	12:36:46.50	62:11:51.3	21.9	20.9	0.16	2.30	0.13	0.000	0.00	0.00	1.00	0.504	21.9	0.16
125	12:37:00.56	62:12:34.6	21.3	22.0	0.35	2.73	0.07	0.000	0.00	0.00	1.00	0.562	21.2	0.35
138	12:36:52.01	62:12:09.6	22.9	21.8	0.14	0.53	0.28	23.42	0.61	0.46	0.31	0.456	22.7	0.62
144	12:36:57.21	62:12:25.8	22.3	22.5	0.09	0.84	0.66	22.28	0.49	0.18	0.02	0.561	22.0	0.80
183	12:36:41.33	62:11:41.0	22.4	23.7	0.09	10.7	0.10	21.24	0.26	0.39	0.15	0.585	22.5	0.40
191	12:36:45.33	62:11:54.4	23.0	23.4	0.30	4.64	0.21	0.000	0.00	0.00	1.00	0.372	22.8	0.30
197	12:36:45.05	62:11:54.1	24.2	26.4	0.12	8.75	0.23	23.21	0.30	0.07	0.03	0.920 ^a	23.8	0.49
205	12:36:47.50	62:12:02.5	24.4	24.1	0.40	0.43	0.49	0.000	0.00	0.00	-1.00	0.920 ^a	24.4	0.40
218	12:36:46.26	62:11:59.7	24.4	0.00	0.00	0.00	0.00	23.28	0.39	0.65	0.00	0.440 ^a	24.4	0.59
220	12:36:52.68	62:12:19.6	23.2	21.6	0.20	0.90	0.33	0.000	0.00	0.00	1.00	0.401	22.9	0.20
245	12:36:46.54	62:12:03.1	24.3	26.1	0.55	0.68	0.38	20.74	0.09	0.50	0.32	0.454	24.2	0.21
247	12:36:45.95	62:12:01.3	23.7	23.0	0.41	0.47	0.54	0.000	0.00	0.00	-1.00	0.679	23.4	0.41
257	12:36:51.72	62:12:20.1	21.5	0.00	0.00	0.00	0.00	19.77	0.30	0.63	0.00	0.401	21.4	0.46
270	12:36:44.82	62:12:00.2	22.9	23.0	0.09	0.85	0.42	22.67	0.42	0.24	0.05	0.457	22.7	0.67
273	12:36:50.16	62:12:16.9	22.4	0.00	0.00	0.00	0.00	20.86	0.41	0.80	0.00	0.905	22.5	0.58
285	12:36:48.65	62:12:14.1	24.4	24.4	0.51	0.72	0.58	0.000	0.00	0.00	-1.00	0.800 ^a	24.3	0.51
310	12:36:48.12	62:12:14.8	24.4	22.2	0.13	0.77	0.35	0.000	0.00	0.00	1.00	0.962	24.5	0.13
319	12:36:49.52	62:12:20.0	24.4	23.7	0.35	0.93	0.58	0.000	0.00	0.00	-1.00	0.961	24.2	0.35
335	12:36:53.45	62:12:34.2	22.8	24.2	0.25	1.28	0.78	20.94	0.31	0.62	0.03	0.559	22.4	0.51
339	12:36:49.05	62:12:21.2	22.4	26.0	0.32	1.62	0.43	21.77	0.31	0.14	-0.03	0.953	22.4	0.51
344	12:36:50.85	62:12:27.2	24.2	24.2	0.39	0.49	0.33	0.000	0.00	0.00	-1.00	0.640 ^a	24.2	0.39
345	12:36:56.65	62:12:45.3	20.0	21.2	0.27	1.06	0.10	22.15	1.89	0.63	0.19	0.517	19.6	2.49
350	12:36:58.77	62:12:52.3	21.2	21.9	0.08	1.46	0.64	21.36	0.48	0.32	0.02	0.320	21.3	0.79
351	12:36:58.32	62:12:51.1	24.0	24.9	0.15	1.55	0.12	23.51	0.49	0.52	0.10	0.240 ^a	23.7	0.74
363	12:36:49.99	62:12:26.2	24.4	0.00	0.00	0.00	0.00	21.74	0.23	0.78	0.00	0.010 ^a	24.5	0.38
381	12:36:55.57	62:12:45.4	21.9	20.8	0.06	0.50	0.11	21.31	0.31	0.22	0.09	0.790	22.0	0.47
391	12:36:41.94	62:12:05.4	21.0	0.00	0.00	0.00	0.00	19.90	0.26	0.06	0.00	0.432	20.8	0.46
394	12:36:58.35	62:12:56.2	24.2	0.00	0.00	0.00	0.00	22.25	0.19	0.49	0.00	0.520 ^a	24.5	0.31
409	12:36:55.62	62:12:49.2	22.9	23.9	0.12	0.61	0.46	23.56	0.62	0.31	0.03	0.950	22.9	1.01
424	12:36:40.95	62:12:05.3	23.2	22.0	0.14	2.48	0.14	0.000	0.00	0.00	1.00	0.882	23.3	0.13
445	12:36:58.07	62:13:00.3	22.3	21.8	0.25	0.89	0.10	23.78	0.95	0.60	0.63	0.319	21.8	0.39
450	12:36:55.26	62:12:52.5	24.2	22.9	0.01	10.2	0.99	22.93	0.41	0.77	0.00	0.720 ^a	24.4	0.68
454	12:36:56.93	62:12:58.1	23.5	0.00	0.00	0.00	0.00	21.25	0.21	0.54	0.00	0.520	23.4	0.35
458	12:36:57.31	62:12:59.6	21.3	23.9	0.48	2.37	0.88	20.66	0.27	0.08	0.05	0.473	21.5	0.45
465	12:36:43.62	62:12:18.2	22.7	0.00	0.00	0.00	0.00	20.70	0.19	0.31	0.00	0.750	22.6	0.31
467	12:36:42.91	62:12:16.3	20.7	21.8	0.52	0.45	0.36	21.48	0.40	0.38	0.62	0.454	20.9	0.56
476	12:36:47.28	62:12:30.6	22.7	22.8	0.38	1.08	0.68	23.51	0.68	0.25	0.32	0.421	22.2	0.80
477	12:36:50.21	62:12:39.7	20.6	25.0	0.20	10.0	0.14	20.88	0.60	0.26	-0.03	0.474	20.2	0.99
495	12:36:41.48	62:12:14.9	23.4	20.1	0.06	1.44	0.69	20.66	0.13	0.43	0.28	0.880 ^a	23.3	0.15
500	12:36:53.90	62:12:53.9	20.8	20.5	0.09	1.15	0.58	20.83	0.43	0.27	0.06	0.642	20.9	0.68
512	12:36:54.78	62:12:58.2	24.3	24.1	0.34	0.51	0.32	0.000	0.00	0.00	-1.00	0.851	24.4	0.34
521	12:36:39.43	62:12:11.7	23.8	23.0	0.20	3.41	0.25	0.000	0.00	0.00	1.00	1.000 ^a	23.5	0.19
524	12:36:50.26	62:12:45.7	21.4	22.2	0.23	6.31	0.22	21.46	0.38	0.38	0.50	0.678	21.3	0.46
537	12:36:47.04	62:12:36.8	20.9	20.8	0.19	0.98	0.36	21.36	0.40	0.09	0.32	0.321	21.0	0.44
549	12:36:55.16	62:13:03.6	23.5	21.7	0.14	2.05	0.29	0.000	0.00	0.00	1.00	0.952	23.3	0.13
563	12:36:50.84	62:12:51.4	23.1	26.5	0.16	5.17	0.28	23.54	0.80	0.26	0.01	0.485	22.3	1.33

HD F {N & HD F {S Quantitative Morphological Analysis 5

(1) ID	(2) R A .(J2000) (h m s)	(3) D .(J2000) (m s)	(4) I ₈₁₄ (cat) m ag	(5) e _{p,b} m ag/ ²	(6) r _{e,p,b} (")	(7) n b	(8) d (0) m ag/ ²	(9) h (")	(10) d m ag/ ²	(11) h (")	(12) B /T	(13) z	(14) I ₈₁₄ (m od) m ag	(15) r _e (")
565	12:36:48.99	62:12:45.8	23.6	23.4	0.41	0.66	0.48	0.000	0.00	0.00	-1.00	0.512	23.5	0.41
581	12:36:49.47	62:12:48.7	23.9	22.6	0.12	0.61	0.03	22.91	0.21	0.16	0.45	0.760 ^a	23.8	0.19
599	12:36:57.71	62:13:15.1	23.0	24.1	0.51	1.16	0.05	0.000	0.00	0.00	-1.00	0.952	22.8	0.51
611	12:36:50.82	62:12:55.8	22.5	22.3	0.12	2.03	0.37	20.92	0.30	0.49	0.13	0.319	22.1	0.44
617	12:36:38.97	62:12:19.7	22.2	23.2	0.48	0.98	0.05	0.000	0.00	0.00	-1.00	0.609	22.2	0.48
619	12:36:55.46	62:13:11.1	22.1	24.3	0.72	3.98	0.05	0.000	0.00	0.00	1.00	0.370	21.7	0.72
631	12:36:55.15	62:13:11.3	23.6	22.4	0.23	0.51	0.17	0.000	0.00	0.00	-1.00	0.321	23.4	0.23
637	12:36:51.43	62:13:00.6	22.7	25.0	0.89	0.70	0.23	0.000	0.00	0.00	-1.00	0.089	22.9	0.89
650	12:36:44.18	62:12:40.3	23.3	23.6	0.08	1.08	0.11	23.12	0.47	0.05	0.03	0.873	22.7	0.76
653	12:36:46.12	62:12:46.4	22.3	21.0	0.10	2.20	0.08	22.73	0.43	0.25	0.45	0.900	22.2	0.33
655	12:36:49.63	62:12:57.5	21.9	0.00	0.00	0.00	0.00	20.06	0.26	0.59	0.00	0.477	21.9	0.42
662	12:36:55.00	62:13:14.7	23.8	23.7	0.22	0.37	0.23	22.02	0.22	0.63	0.35	0.511	23.9	0.29
669	12:36:39.77	62:12:28.5	23.7	0.00	0.00	0.00	0.00	22.31	0.26	0.25	0.00	0.010 ^a	23.6	0.37
671	12:36:47.54	62:12:52.6	23.9	0.00	0.00	0.00	0.00	22.07	0.32	0.66	0.00	0.681	23.6	0.55
683	12:36:41.61	62:12:35.6	24.4	22.6	0.13	1.76	0.24	0.000	0.00	0.00	1.00	0.520 ^a	24.3	0.12
689	12:36:39.86	62:12:31.5	24.1	21.9	0.11	0.66	0.60	23.07	0.32	0.52	0.30	0.640 ^a	23.9	0.34
694	12:36:43.15	62:12:42.2	21.7	23.2	0.57	5.70	0.25	0.000	0.00	0.00	1.00	0.847	21.2	0.56
709	12:36:44.18	62:12:47.8	21.6	21.7	0.10	1.79	0.20	21.25	0.36	0.20	0.11	0.558	21.5	0.53
716	12:36:38.40	62:12:31.3	22.6	0.00	0.00	0.00	0.00	21.87	0.58	0.77	0.00	0.944	22.6	0.90
719	12:36:49.68	62:13:07.3	24.2	24.2	0.18	0.85	0.32	22.51	0.17	0.18	0.25	0.920 ^a	24.2	0.25
720	12:36:43.96	62:12:50.0	20.9	23.7	0.37	1.79	0.60	20.58	0.53	0.60	-0.06	0.557	20.8	0.85
727	12:36:38.60	62:12:33.8	23.9	24.4	0.06	2.85	0.61	21.95	0.30	0.66	0.02	0.904	23.7	0.49
740	12:36:49.03	62:13:09.7	24.0	21.9	0.18	0.46	0.44	0.000	0.00	0.00	1.00	0.960 ^a	23.8	0.18
743	12:36:49.37	62:13:11.2	22.1	21.3	0.20	2.50	0.15	0.000	0.00	0.00	1.00	0.478	21.8	0.19
746	12:36:49.72	62:13:13.0	21.4	24.5	0.77	1.34	0.70	21.09	0.57	0.70	0.13	0.475	21.4	0.93
749	12:36:50.47	62:13:16.1	22.6	22.6	0.04	17.0	0.62	22.39	0.67	0.71	0.03	0.851	22.6	1.09
751	12:36:48.08	62:13:09.0	20.4	19.1	0.10	1.52	0.04	21.58	0.57	0.08	0.41	0.475	20.2	0.42
757	12:36:51.05	62:13:20.6	19.6	21.7	0.28	0.58	0.60	20.99	1.29	0.60	0.03	0.199	19.3	2.10
774	12:36:44.58	62:13:04.6	21.2	19.7	0.05	2.32	0.72	20.53	0.53	0.71	0.05	0.485	21.1	0.84
775	12:36:48.47	62:13:16.6	23.2	22.2	0.17	0.99	0.48	23.15	0.32	0.09	0.41	0.474	23.1	0.32
780	12:36:48.78	62:13:18.4	22.6	23.2	0.07	0.62	0.14	23.12	0.64	0.25	0.02	0.749	22.3	1.05
781	12:36:46.75	62:13:12.3	23.6	23.2	0.09	0.77	0.40	22.32	0.38	0.63	0.07	0.600 ^a	23.4	0.59
782	12:36:45.61	62:13:08.9	23.6	22.6	0.18	2.20	0.18	0.000	0.00	0.00	1.00	0.480 ^a	23.4	0.17
793	12:36:49.07	62:13:21.8	24.4	23.5	0.30	0.40	0.05	0.000	0.00	0.00	-1.00	0.880 ^a	23.8	0.30
798	12:36:46.15	62:13:13.8	24.2	21.6	0.11	1.14	0.31	0.000	0.00	0.00	1.00	0.640 ^a	24.1	0.11
810	12:36:42.51	62:13:05.1	24.3	24.5	0.25	3.00	0.20	0.000	0.00	0.00	-1.00	0.720 ^a	24.5	0.25
817	12:36:42.72	62:13:07.1	22.1	28.4	1.88	10.0	0.67	19.82	0.24	0.74	0.20	0.485	22.2	0.44
866	12:36:47.45	62:13:30.0	23.5	0.00	0.00	0.00	0.00	22.57	0.26	0.02	0.00	0.960 ^a	23.5	0.37
869	12:36:45.86	62:13:25.8	20.9	24.8	0.32	1.55	0.51	21.96	0.84	0.28	0.01	0.321	20.6	1.39
876	12:36:45.41	62:13:25.9	22.6	20.1	0.10	3.04	0.67	20.34	0.18	0.52	0.43	0.441	22.2	0.21
882	12:36:52.23	62:13:48.0	24.3	22.8	0.10	0.68	0.23	0.000	0.00	0.00	1.00	0.520 ^a	24.2	0.19
884	12:36:54.10	62:13:54.3	22.4	0.00	0.00	0.00	0.00	21.46	0.32	0.29	0.00	0.849	22.3	0.54
888	12:36:55.59	62:13:59.8	23.7	22.3	0.03	6.45	0.10	22.41	0.40	0.72	0.07	0.559	23.6	0.62
890	12:36:42.37	62:13:19.3	23.8	21.6	0.10	2.51	0.24	0.000	0.00	0.00	1.00	0.760 ^a	23.8	0.09
899	12:36:55.50	62:14:02.6	22.9	0.00	0.00	0.00	0.00	21.48	0.47	0.80	0.00	0.564	22.8	0.80
902	12:36:42.02	62:13:21.4	23.5	21.0	0.09	1.25	0.64	22.77	0.20	0.05	0.46	0.846	23.6	0.18
912	12:36:51.80	62:13:53.8	21.1	21.8	0.56	0.58	0.60	22.25	0.86	0.60	-0.49	0.557	20.8	0.82
914	12:36:49.44	62:13:46.9	18.1	19.4	0.56	2.40	0.40	0.000	0.00	0.00	1.00	0.089	18.1	0.55
915	12:36:48.03	62:13:43.0	24.3	24.8	0.15	0.45	0.60	23.80	0.55	0.60	0.04	0.840 ^a	24.0	0.88
938	12:36:51.98	62:14:00.8	23.0	0.00	0.00	0.00	0.00	21.02	0.32	0.67	0.00	0.557	22.7	0.53
941	12:36:52.87	62:14:04.8	23.2	25.1	0.19	1.52	0.14	21.96	0.21	0.05	-0.08	0.498	23.3	0.33
979	12:36:53.65	62:14:17.6	23.4	0.00	0.00	0.00	0.00	21.36	0.33	0.73	0.00	0.517	23.2	0.48
989	12:36:49.50	62:14:06.7	21.8	21.1	0.18	0.61	0.48	21.29	0.36	0.31	0.25	0.752	21.6	0.44
990	12:36:46.03	62:13:56.3	24.2	0.00	0.00	0.00	0.00	21.93	0.16	0.31	0.00	1.000 ^a	24.2	0.25
1018	12:36:46.35	62:14:04.6	21.2	24.8	1.13	11.0	0.05	0.000	0.00	0.00	1.00	0.960	20.6	1.12
1022	12:36:51.39	62:14:20.9	23.3	0.00	0.00	0.00	0.00	22.05	0.53	0.60	0.00	0.439	22.8	0.88
1027	12:36:48.35	62:14:12.3	23.8	24.2	0.88	0.43	0.80	0.000	0.00	0.00	-1.00	0.920 ^a	23.9	0.88
1028	12:36:50.36	62:14:18.6	23.0	23.1	0.18	0.79	0.84	22.45	0.39	0.37	0.05	0.816	22.9	0.62
1029	12:36:46.54	62:14:07.5	23.9	22.7	0.20	1.54	0.33	0.000	0.00	0.00	1.00	0.130	23.7	0.19
1038	12:36:48.10	62:14:14.4	24.4	21.8	0.06	0.57	0.24	22.03	0.15	0.37	0.29	0.920 ^a	24.3	0.16
1048	12:36:47.18	62:14:14.2	23.5	23.1	0.15	0.53	0.49	21.06	0.18	0.43	0.11	0.609	23.2	0.27
1063	12:36:53.11	62:14:38.0	24.2	23.5	0.37	0.85	0.60	0.000	0.00	0.00	-1.00	0.400 ^a	24.0	0.37
1067	12:36:48.32	62:14:26.2	19.1	19.8	0.18	1.02	0.20	19.40	0.48	0.20	0.15	0.139	19.0	0.68

(1) ID	(2) R A .(J2000) (h m s)	(3) D .(J2000) (° m s)	(4) I _{B14} (cat) m ag	(5) e _p m ag/ ²	(6) r _{e,p} (")	(7) n	(8) b	(9) a (0) m ag/" ²	(10) h (")	(11) d	(12) B / T	(13) z	(14) I _{B14} (mod) m ag	(15) r _e (")
H D F {S}														
29	22:32:46.27	-60:34:16.3	21.0	19.3	0.09	0.49	0.23	20.19	0.19	0.03	-0.36	0.460 ^a	21.2	0.19
30	22:33:00.48	-60:34:17.6	23.2	24.3	0.45	4.82	0.29	0.000	0.00	0.00	1.00	0.620 ^a	22.9	0.45
41	22:32:56.06	-60:34:14.1	22.1	21.4	0.22	0.50	0.47	22.32	0.45	0.33	0.39	0.564	22.0	0.42
49	22:32:45.60	-60:34:15.1	24.4	24.8	0.50	2.04	0.41	0.000	0.00	0.00	-1.00	0.462	23.8	0.50
50	22:32:47.55	-60:34:08.5	21.2	0.00	0.00	0.00	0.00	20.53	0.34	0.23	0.00	0.560	21.2	0.60
53	22:32:50.94	-60:34:15.2	24.2	0.00	0.00	0.00	0.00	20.51	0.09	0.19	0.00	0.424	23.8	0.15
64	22:32:55.21	-60:34:10.0	23.4	0.00	0.00	0.00	0.00	21.99	0.22	0.05	0.00	0.960 ^a	23.3	0.32
65	22:33:01.54	-60:34:10.7	23.5	24.7	0.13	0.79	0.63	21.50	0.20	0.41	0.02	0.853	23.5	0.33
75	22:32:55.23	-60:34:07.4	23.1	23.9	0.10	0.83	0.35	22.69	0.38	0.20	0.03	0.465	22.9	0.62
87	22:33:04.44	-60:34:09.0	24.0	24.0	0.18	0.69	0.10	23.13	0.31	0.29	0.22	0.480 ^a	23.7	0.41
91	22:32:52.22	-60:34:02.6	22.0	21.8	0.11	0.72	0.27	20.44	0.26	0.63	0.13	0.511	22.3	0.37
95	22:32:45.98	-60:34:07.2	23.8	0.00	0.00	0.00	0.00	19.53	0.07	0.25	0.00	0.753	23.6	0.12
97	22:32:48.89	-60:34:04.6	22.6	20.7	0.09	3.36	0.03	0.000	0.00	0.00	1.00	0.980 ^a	22.5	0.09
99	22:32:52.13	-60:33:59.3	21.8	23.5	0.23	1.47	0.50	21.94	0.86	0.59	0.04	0.564	21.1	1.38
138	22:32:46.88	-60:33:54.7	21.2	20.2	0.19	3.07	0.42	0.000	0.00	0.00	1.00	0.420 ^a	21.1	0.19
153	22:32:48.23	-60:33:54.9	23.4	0.00	0.00	0.00	0.00	21.93	0.39	0.64	0.00	0.721	23.1	0.54
184	22:33:03.56	-60:33:41.6	20.0	23.6	0.37	3.49	0.28	19.86	0.43	0.25	-0.07	0.340	19.8	0.71
186	22:33:05.77	-60:33:41.5	20.0	22.8	0.72	7.84	0.05	0.000	0.00	0.00	1.00	0.328	19.8	0.71
189	22:32:57.87	-60:33:49.1	23.6	23.2	0.17	0.92	0.83	23.37	0.71	0.60	0.05	0.428	23.0	1.13
193	22:32:47.64	-60:33:35.7	19.5	20.7	0.19	3.08	0.18	20.20	0.58	0.27	0.19	0.580	19.4	0.82
198	22:33:02.44	-60:33:46.5	22.3	22.2	0.14	0.48	0.27	22.51	0.47	0.37	-0.16	0.695	22.4	0.66
215	22:32:47.47	-60:33:43.9	24.2	0.00	0.00	0.00	0.00	21.68	0.13	0.07	0.00	0.560 ^a	24.1	0.24
220	22:32:49.42	-60:33:43.6	24.2	0.00	0.00	0.00	0.00	21.04	0.10	0.25	0.00	0.647	24.3	0.16
223	22:32:53.73	-60:33:37.4	21.5	24.0	0.35	0.99	0.10	22.83	0.88	0.15	0.09	0.565	21.1	1.34
227	22:32:59.42	-60:33:39.6	22.1	0.00	0.00	0.00	0.00	21.88	0.43	0.28	0.00	0.464	22.0	0.73
234	22:32:51.50	-60:33:37.4	22.0	22.0	0.07	1.48	0.92	19.77	0.18	0.45	-0.01	0.577	22.1	0.30
244	22:32:54.67	-60:33:33.0	21.2	22.1	0.02	1.29	0.42	20.15	0.52	0.75	0.01	0.173	21.0	0.87
247	22:32:45.30	-60:33:32.4	21.5	20.8	0.19	2.92	0.26	0.000	0.00	0.00	1.00	0.520 ^a	21.5	0.19
256	22:32:58.21	-60:33:31.5	22.0	0.00	0.00	0.00	0.00	21.51	0.37	0.25	0.00	0.423	21.9	0.60
265	22:32:55.72	-60:33:33.6	23.8	24.5	0.02	12.0	0.10	23.81	0.54	0.23	0.00	0.564	23.4	0.54
270	22:32:52.34	-60:33:32.9	22.7	0.00	0.00	0.00	0.00	19.48	0.11	0.23	0.00	0.500 ^a	22.5	0.17
273	22:33:02.12	-60:33:34.9	24.1	23.4	0.08	1.51	0.10	23.18	0.57	0.65	0.08	0.500 ^a	23.4	0.89
283	22:32:55.81	-60:33:30.2	24.0	0.00	0.00	0.00	0.00	22.92	0.51	0.62	0.00	0.180 ^a	23.4	0.89
288	22:33:04.25	-60:33:31.8	24.0	0.00	0.00	0.00	0.00	22.62	0.25	0.05	0.00	0.465	23.6	0.40
292	22:33:02.75	-60:33:22.0	20.2	20.1	0.20	1.75	0.36	21.40	0.72	0.57	0.48	0.464	20.3	0.53
297	22:32:57.08	-60:33:28.8	23.9	22.5	0.12	1.60	0.29	24.44	0.47	0.01	0.39	0.680 ^a	23.5	0.41
301	22:32:59.45	-60:33:28.8	24.2	22.4	0.13	1.51	0.64	21.63	0.16	0.51	0.35	0.980 ^a	23.8	0.22
306	22:33:00.86	-60:33:25.6	23.6	24.5	0.48	0.92	0.41	0.000	0.00	0.00	-1.00	0.940 ^a	23.9	0.48
307	22:32:50.55	-60:33:25.8	22.6	26.4	0.13	2.71	0.10	21.36	0.29	0.29	0.01	0.440 ^a	22.4	0.48
314	22:32:52.15	-60:33:23.8	22.8	0.00	0.00	0.00	0.00	20.79	0.16	0.14	0.00	0.220 ^a	22.8	0.25
317	22:32:57.04	-60:33:22.9	22.8	20.8	0.09	2.61	0.16	0.000	0.00	0.00	1.00	0.520 ^a	22.9	0.09
337	22:32:45.77	-60:32:50.4	22.1	0.00	0.00	0.00	0.00	21.81	0.33	0.06	0.00	0.852	22.3	0.53
339	22:32:54.04	-60:32:51.6	22.1	20.7	0.14	1.51	0.10	21.70	0.32	0.37	0.62	0.515	21.5	0.23
344	22:32:47.66	-60:32:52.2	23.3	25.3	0.07	1.14	0.90	22.18	0.38	0.52	0.01	0.480 ^a	23.0	0.64
345	22:32:49.23	-60:32:53.3	22.5	24.3	0.22	1.98	0.11	22.76	0.58	0.03	0.08	0.500 ^a	21.8	0.90
367	22:32:47.77	-60:32:55.9	24.2	26.7	0.07	10.5	0.10	23.96	0.42	0.21	-0.04	0.960 ^a	24.0	0.07
374	22:33:00.48	-60:32:58.4	24.1	0.00	0.00	0.00	0.00	20.68	0.10	0.20	0.00	0.440 ^a	23.9	0.14
394	22:32:45.63	-60:33:01.3	21.4	0.00	0.00	0.00	0.00	19.81	0.24	0.40	0.00	0.760 ^a	21.4	0.41
409	22:32:57.53	-60:33:06.0	20.4	21.9	0.05	4.38	0.01	20.71	0.40	0.01	-0.02	0.580	20.6	0.66
410	22:32:57.21	-60:33:05.4	22.8	0.00	0.00	0.00	0.00	22.00	0.40	0.46	0.00	0.582	22.7	0.56
415	22:32:54.01	-60:33:05.4	22.7	0.00	0.00	0.00	0.00	20.42	0.29	0.72	0.00	0.581	22.4	0.49
420	22:32:51.66	-60:33:05.9	24.3	23.2	0.16	3.31	0.14	0.000	0.00	0.00	1.00	0.980 ^a	24.1	0.16
427	22:32:52.29	-60:33:08.3	21.1	21.4	0.09	0.63	0.61	21.74	0.64	0.53	0.03	0.583	21.5	1.05
429	22:33:03.85	-60:33:08.7	22.9	25.1	0.16	12.4	0.10	22.69	0.45	0.46	0.13	0.970	22.9	0.71
438	22:32:48.99	-60:33:09.2	24.6	0.00	0.00	0.00	0.00	22.17	0.22	0.57	0.00	0.359	24.3	0.36
442	22:32:49.49	-60:33:11.0	23.1	23.9	0.33	1.24	0.14	23.94	0.72	0.33	0.36	0.564	22.5	0.78
446	22:32:53.91	-60:33:13.3	21.0	22.6	0.26	4.05	0.06	20.10	0.39	0.40	0.33	0.364	20.4	0.54
456	22:32:50.97	-60:33:13.9	24.4	22.2	0.04	3.75	0.10	22.67	0.35	0.61	0.15	0.460 ^a	23.7	0.51
459	22:32:48.55	-60:33:13.8	23.3	0.00	0.00	0.00	0.00	19.20	0.07	0.29	0.00	0.480 ^a	23.1	0.14
464	22:33:01.88	-60:33:16.3	21.7	24.1	0.57	2.32	0.88	20.13	0.26	0.52	0.07	0.428	21.7	0.45
476	22:32:55.86	-60:33:17.6	23.0	25.6	0.11	12.7	0.47	21.35	0.20	0.19	0.04	0.581	23.0	0.33
482	22:33:00.14	-60:33:18.9	23.3	21.8	0.11	0.83	0.28	22.68	0.28	0.02	0.31	0.540	23.0	0.30

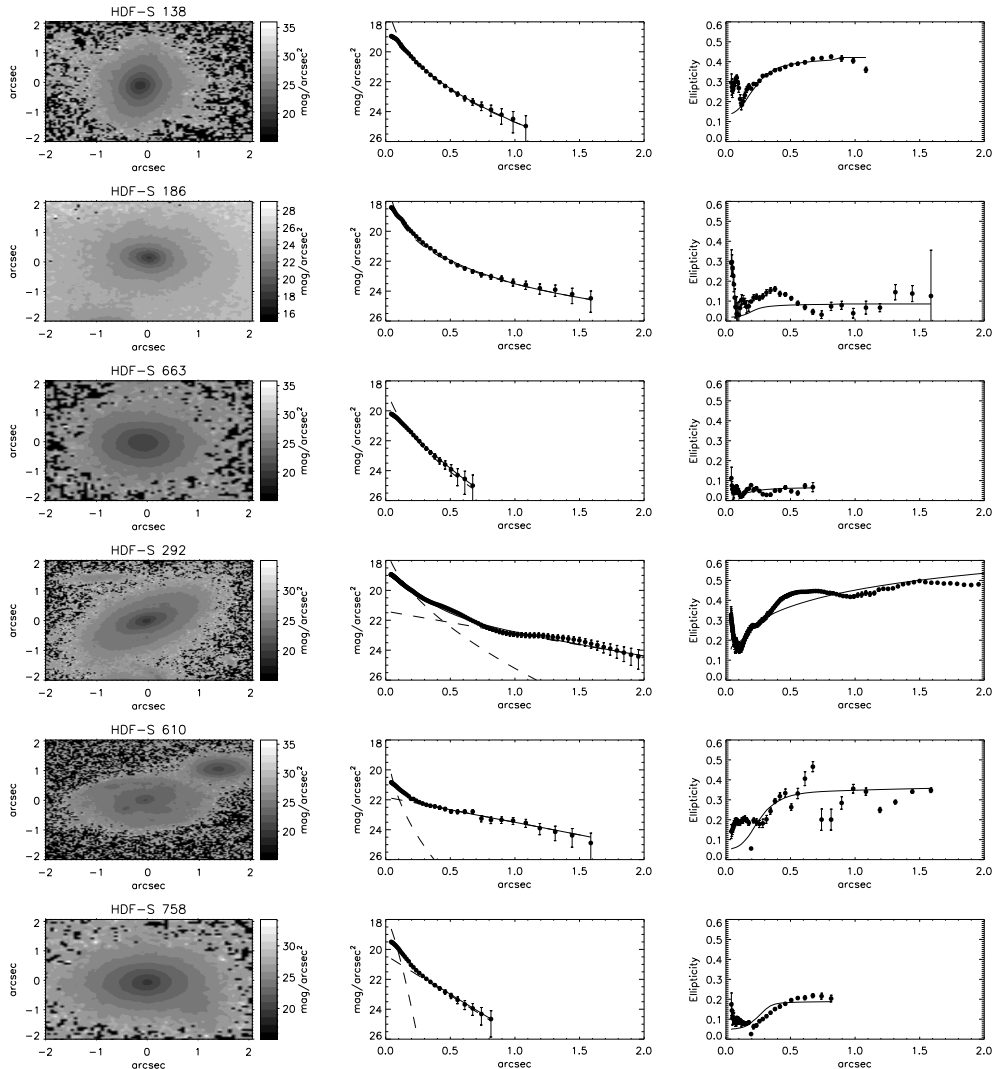


Figure 1. Surface brightness and ellipticity semi-major radial profiles fitting to some galaxies in our sample. The three top galaxies are well fitted with a single Sersic law. The three bottom galaxies are fitted using a Sersic bulge plus an exponential disc.

A preliminary way of examining the goodness of our structural parameter determination is to compare the best model magnitude with the magnitude measured in a model independent way (Fig. 2). The model independent magnitude is the catalogs' magnitude. As expected from its extrapolation to the infinity, the model magnitude is almost always equal or brighter than the model independent determination.

4 OBJECT MORPHOLOGICAL CLASSIFICATION

Following previous works (e.g. M98) our galaxy classification scheme relies on B/T (Simien & de Vaucouleurs 1986). Galaxies are considered "ellipticals" if their $B/T > 0.6$. If this is the situation the galaxies are reanalysed with just a Sersic

component and the parameters provided here correspond to this case. Galaxies with B/T between 0.5–0.6 are classified as S0 and objects with $B/T < 0.5$ are named "spirals". However, there is a group of objects that can not be well fitted by our models. These objects have peculiar shapes (and consequently, their isophotes are hardly fitted by ellipses) and are classified in the Irr/Merger category. These objects are indicated in Tables 1 and 2 with $B/T = -1$. In addition, there are a group of visually classified spiral galaxies where a reliable fit is not achieved due to the presence of strong secondary structures as bars, spiral arms, etc. These galaxies are indicated with a value of $B/T < 0$.

The results of our galaxy classification are shown in Table 3. There are some discrepancies between the number of galaxies classified as E/S0 and Sa/Sc in the HDF{S and

(1) ID	(2) R A .(J2000) (h m s)	(3) D .(J2000) (m s)	(4) I ₈₁₄ (cat) m ag	(5) e _p m ag/ ²	(6) r _{e,p} ("	(7) n	(8) b	(9) d (0) m ag/" ²	(10) h ()	(11) d ()	(12) B /T	(13) z	(14) I ₈₁₄ (m od) m ag	(15) r _e ()
487	22:32:52.25	-60:33:19.3	24.0	23.5	0.34	0.33	0.19	0.000	0.00	0.00	-1.00	0.240 ^a	23.7	0.34
490	22:32:54.27	-60:33:20.1	23.8	0.00	0.00	0.00	0.00	22.68	0.33	0.60	0.00	0.565	24.0	0.51
491	22:32:54.33	-60:33:20.6	23.8	0.00	0.00	0.00	0.00	22.43	0.31	0.56	0.00	0.565	23.8	0.47
508	22:32:45.39	-60:33:23.0	23.9	23.1	0.26	0.47	0.20	0.000	0.00	0.00	-1.00	0.280 ^a	23.9	0.26
528	22:32:53.63	-60:32:35.9	21.1	24.1	0.09	13.0	0.59	20.66	0.54	0.64	0.02	0.365	21.0	0.90
544	22:32:59.43	-60:32:40.1	22.7	25.2	0.07	10.5	0.10	21.67	0.60	0.81	0.01	0.480 ^a	22.5	1.01
549	22:32:50.90	-60:32:42.9	20.8	19.9	0.14	1.57	0.13	22.32	0.56	0.19	0.60	0.579	20.7	0.27
575	22:32:55.75	-60:32:13.4	24.1	25.9	0.18	0.43	0.10	23.18	0.34	0.20	0.03	0.759	23.6	0.56
577	22:32:53.09	-60:32:38.9	23.7	23.4	0.09	1.11	0.49	21.84	0.27	0.51	0.05	0.540 ^a	23.3	0.44
578	22:32:52.07	-60:31:41.0	23.1	23.8	0.23	1.41	0.32	22.16	0.40	0.51	0.18	0.512	22.7	0.57
599	22:32:50.80	-60:31:41.6	23.5	0.00	0.00	0.00	0.00	22.06	0.26	0.42	0.00	0.515	23.5	0.45
601	22:32:54.08	-60:31:42.7	22.8	23.8	0.00	10.4	0.37	20.39	0.17	0.19	0.01	0.513	22.4	0.28
609	22:32:57.75	-60:32:33.0	21.9	26.3	0.50	10.1	0.28	19.96	0.18	0.33	0.12	0.517	21.8	0.32
610	22:32:57.97	-60:32:34.3	21.3	21.3	0.07	2.24	0.17	21.83	0.64	0.42	0.08	0.760	21.2	0.99
635	22:32:56.06	-60:31:48.9	21.3	25.5	1.25	11.9	0.96	21.74	0.61	0.30	-0.03	0.514	21.1	1.03
638	22:32:52.69	-60:31:53.2	24.1	0.00	0.00	0.00	0.00	21.81	0.33	0.77	0.00	0.940 ^a	23.8	0.50
645	22:32:57.13	-60:31:52.2	22.3	0.00	0.00	0.00	0.00	20.05	0.23	0.36	0.00	0.600 ^a	21.8	0.38
663	22:32:50.28	-60:32:03.3	22.2	21.3	0.17	1.82	0.09	0.000	0.00	1.00	0.414	22.2	0.17	
673	22:32:55.53	-60:32:17.4	23.3	22.5	0.19	0.68	0.53	23.06	0.46	0.37	0.26	0.519	22.9	0.55
676	22:32:50.80	-60:31:59.7	24.2	22.8	0.23	0.50	0.33	0.000	0.00	-1.00	0.318	24.0	0.23	
684	22:32:55.71	-60:32:11.4	21.5	19.6	0.06	0.97	0.00	20.57	0.29	0.31	0.25	0.673	21.3	0.35
687	22:32:50.34	-60:32:01.1	24.3	28.9	0.08	3.33	0.10	23.20	0.38	0.50	0.01	0.920 ^a	24.0	0.63
691	22:32:48.83	-60:32:03.5	24.1	22.4	0.14	1.40	0.15	0.000	0.00	1.00	0.980 ^a	24.0	0.14	
708	22:32:52.70	-60:32:07.2	21.8	24.7	0.76	2.63	0.45	21.91	0.47	0.28	0.29	0.464	21.5	0.78
758	22:32:54.77	-60:32:15.4	21.6	19.1	0.06	0.75	0.11	20.39	0.20	0.19	0.36	0.480 ^a	21.6	0.18
759	22:32:53.85	-60:32:13.1	24.2	24.6	0.30	1.12	0.87	22.31	0.27	0.39	0.06	0.114	23.6	0.44
763	22:33:00.23	-60:32:33.9	20.5	0.00	0.00	0.00	0.00	20.57	0.45	0.29	0.00	0.415	20.7	0.77
766	22:32:56.04	-60:32:20.4	22.5	23.8	0.21	0.67	0.23	22.73	0.72	0.43	0.05	0.519	21.9	1.16
768	22:32:53.04	-60:32:17.0	23.7	24.0	0.21	1.54	0.29	23.82	1.04	0.71	0.16	0.760 ^a	22.9	1.45
770	22:32:48.87	-60:32:16.0	23.0	25.1	0.31	2.08	0.44	21.41	0.31	0.61	0.10	0.580	22.8	0.51
774	22:32:52.01	-60:32:14.9	23.4	0.00	0.00	0.00	0.00	22.00	0.30	0.39	0.00	0.800 ^a	23.2	0.52
822	22:32:54.78	-60:32:28.9	24.1	24.4	0.11	1.51	0.10	23.70	0.41	0.06	0.08	0.760 ^a	23.5	0.64
10010	22:33:05.87	-60:33:43.3	22.6	22.4	0.37	0.54	0.27	0.000	0.00	-1.00	0.640 ^a	22.4	0.37	

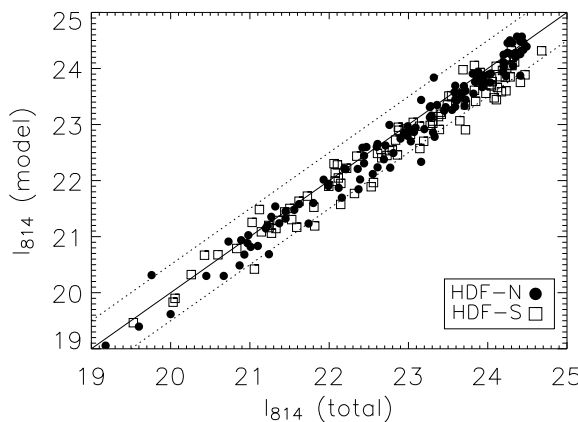


Figure 2. The total magnitude retrieved from the fitting model is compared to the total magnitude measured in a model-independent way (catalogs' magnitude) for the galaxies analysed in this paper. Dashed lines corresponds to 0.5 mag over the assumption of an exact agreement.

HDF{N. These differences illustrate the strong field-to-field variations present in small observing volumes.

Table 3. Coarse binning of galaxy classifications.

Type	B/T	HDF{N	HDF{S	Total
E/S0	> 0.5	20%	12%	16%
Sa/Sc	< 0.5	63%	74%	68%
Irr/M erger		17%	14%	16%

5 DETERMINATION OF ACCURACY

To calibrate the accuracy of our parameter determination we have made two different tests. First, we have run our code on simulated artificial galaxies. This permits an evaluation of the apparent magnitude limit cut-off. Galaxies brighter than this magnitude limit are then claimed to be recovered with a certain degree of accuracy. We also have made a direct comparison between the structural parameters recovered using our algorithm and those recovered using GIM2D on the HDF{N (M98). We describe these two issues in the following subsections.

5.1 Simulations

Simulations are a key element in the interpretation of the observations. For fainter objects (i.e. at decreasing the signal

Table 2. F606W Best Morphological Parameter Values For Galaxies with $I_{814}(\text{AB}) < 24.5$ mag and $z < 0.4$ in the HDF{N and HDF{S.

(1) ID	(2) V ₆₀₆ (cat) mag	(3) $r_{\text{e};\text{b}}$ mag/ "^2	(4) $r_{\text{e};\text{b}}$ "	(5) n	(6) b	(7) $d(0)$ mag/ "^2	(8) h "	(9) d "	(10) B/T	(11) z	(12) V ₈₁₄ (mod) mag	(13) r_{e} "
HDF{N												
10	24.4	26.1	0.11	1.35	0.26	23.6	0.44	0.40	0.02	0.080 ^a	23.9	0.72
11	23.6	0.00	0.00	0.00	0.00	22.1	0.33	0.60	0.00	0.321	23.6	0.50
55	23.9	0.00	0.00	0.00	0.00	23.3	0.53	0.75	0.00	0.200 ^a	24.2	0.75
85	20.1	23.1	0.28	1.52	0.10	20.7	0.70	0.40	0.06	0.089	20.0	1.10
191	24.8	25.5	0.37	4.40	0.24	0.00	0.00	0.00	1.00	0.372	24.6	0.37
350	21.8	24.7	0.15	2.58	0.55	21.9	0.53	0.25	0.02	0.320	21.6	0.88
351	24.5	27.3	0.32	2.10	0.30	23.7	0.46	0.54	0.06	0.240 ^a	24.2	0.74
363	24.9	0.00	0.00	0.00	0.00	22.1	0.18	0.60	0.00	0.010 ^a	24.8	0.28
445	22.6	21.7	0.22	0.87	0.53	23.4	0.60	0.56	0.56	0.319	22.5	0.37
537	21.5	21.5	0.24	1.03	0.42	22.4	0.52	0.04	0.36	0.321	21.4	0.55
611	22.8	0.00	0.00	0.00	0.00	20.5	0.28	0.70	0.00	0.319	22.6	0.48
619	24.0	25.9	0.72	4.00	0.23	0.00	0.00	0.00	1.00	0.370	23.9	0.72
631	24.0	22.6	0.22	0.37	0.62	23.4	0.25	0.25	-0.52	0.321	23.9	0.22
637	23.4	26.3	1.66	1.00	0.05	0.00	0.00	0.00	-1.00	0.089	22.6	1.66
669	24.1	0.00	0.00	0.00	0.00	22.6	0.27	0.29	0.00	0.010 ^a	23.9	0.39
757	19.9	21.7	0.18	0.42	0.62	21.3	1.09	0.51	0.02	0.199	19.9	1.79
869	21.5	24.1	0.23	1.62	0.67	22.4	0.64	0.37	0.03	0.321	21.8	1.04
914	18.7	20.3	0.63	2.30	0.23	0.00	0.00	0.00	1.00	0.089	18.5	0.63
1029	24.3	23.2	0.21	1.86	0.40	0.00	0.00	0.00	1.00	0.130	24.1	0.21
1067	19.5	20.0	0.11	0.51	0.18	19.2	0.42	0.34	0.06	0.139	19.5	0.66
HDF{S												
184	20.8	23.6	0.19	6.03	0.32	20.7	0.41	0.27	-0.08	0.340	20.9	0.66
186	20.8	23.7	0.77	6.84	0.04	0.00	0.00	0.00	1.00	0.328	20.6	0.77
244	21.7	0.00	0.00	0.00	0.00	21.0	0.67	0.80	0.00	0.173	21.7	1.00
283	24.4	27.2	0.24	3.11	0.12	23.6	0.59	0.55	0.04	0.180 ^a	23.6	0.96
314	23.5	0.00	0.00	0.00	0.00	21.6	0.18	0.14	0.00	0.220 ^a	23.5	0.28
438	25.1	0.00	0.00	0.00	0.00	22.6	0.23	0.55	0.00	0.359	24.7	0.37
446	21.9	24.0	0.12	12.1	0.09	21.2	0.23	0.44	0.19	0.364	22.8	0.37
487	24.2	24.2	0.43	0.69	0.14	0.00	0.00	0.00	-1.00	0.240 ^a	23.6	0.43
508	24.0	24.3	0.37	0.64	0.51	0.00	0.00	0.00	-1.00	0.280 ^a	24.8	0.37
528	21.7	0.00	0.00	0.00	0.00	21.1	0.45	0.56	0.00	0.365	21.8	0.68
676	24.5	23.4	0.25	1.42	0.39	0.00	0.00	0.00	-1.00	0.318	24.1	0.25
759	24.4	23.8	0.18	0.36	0.26	23.0	0.31	0.48	0.17	0.114	24.0	0.42

to noise S/N) the structural parameters of the galaxies are progressively more difficult to determine. To quantify this effect it is necessary to run realistic simulations matching the observational conditions. We simulated two kind of objects. First, we created bulge only (i.e. pure elliptical) artificial galaxies, and second, we constructed bulge+disc galaxies. In both cases, we made 150 artificial objects with structural parameters randomly distributed in the following ranges:

Bulge only structures: $196 \text{ I(AB)} \leq 25, 0.05 \leq r_e \leq 0.6 \text{"}$, $0.56 \leq n \leq 4$, and $0.6 \leq b \leq 0.6$.

Bulge+disc structures: $196 \text{ I(AB)} \leq 25, 0.05 \leq r_e \leq 0.6 \text{"}$, $0.56 \leq n \leq 4$, and $0.6 \leq b \leq 0.4$, $0.2 \leq h \leq 1.5$, $0.06 \leq B-T \leq 1$, and $0.6 \leq d \leq 0.6$.

Artificial galaxies were created by using the IRAF task M K O B J E C T . We support as an input to this task the surface brightness distribution coming from our detailed convolution between the PSF and the original model. To simulate the real conditions of our observations, we added a background sky image (free of sources) taken from a piece of the

real image. The PSF FWHM in the simulation was set at 0.147" and assumed known exactly. The pixel scale of the simulation was 0.04" , as are the drizzled HDFS pixel scales. The same procedure was used to process both the simulated and actual data.

From these simulations we find that the bulge and disc parameters (as well as the galaxy global properties as total magnitude, r_e , etc.) can be determined with an accuracy of 10% for galaxies with $I_{814}(\text{AB}) < 24.5$ mag. Consequently, we consider $I_{814}(\text{AB}) = 24.5$ mag as our limiting magnitude for a reliable determination of the parameters. Further details of how the simulations are constructed and the errors determined can be found in Trujillo et al. (2001a) and Aguerri & Trujillo (2002).

5.2 Comparison with Previous Works

M98 using a different code, GIM2D (Simard 1998), conducted a quantitative morphological analysis on the HDFS close to that presented here. The main differences between

both analyses are: the limiting apparent magnitude and the model for the bulge component. GIM 2D was run down to $I_{814}(\text{AB}) < 26$ mag, i.e. 1.5 mag deeper than in the present analysis. However, although individual errors for the galaxy parameters are available, there are not simulations showing the accuracy of the structural parameters as a function of the apparent magnitude. Another difference is that GIM 2D was run using a de Vaucouleurs model ($n=4$ fixed) for the bulges. Fixing n to 4 has the advantage of decreasing the number of free parameters, however, in the nearby universe a range of n (from 0.3 to 6) is found (Andredakis, Peltier & Balcells 1995, Graham 2001). Moreover, n relates with the total magnitude of the bulge component and it would be of interest to know if this relation evolves with time (Aguerri & Trujillo 2004).

In Fig. 3 we show the comparison between the global size of the galaxies r_e as obtained from our code (n free) and GIM 2D ($n=4$) versus z and versus the apparent magnitude. The comparison is limited to $I_{814}(\text{AB}) < 24.5$ mag and $z < 1$. There is a good agreement between these two different algorithms (75% of the galaxies have a size difference less than 20%). However, we find a small offset of 5% toward smaller r_e in our code relative to GIM 2D. This offset seems to be real in the sense that a T-Student test rejects the hypothesis that this is produced by chance by more than 99.9%. This offset is not dependent on z or magnitude and (due to it is not present in our simulations) must be intrinsically related to the way our code and GIM 2D estimate the global galaxy size. As explained before our code uses Eq. (5) to estimate r_e . This equation is derived by the definition of effective radius (i.e. $L(r_e) = 0.5L(L)$). On the other hand, GIM 2D evaluates r_e by integrating the bulge and disc expressions out to infinity and then evaluating r_e . It is possible that their assumption of $n=4$ plays here this minor role including more light than what it is actually observed with a smaller r_e . In any case, it is important to note that this offset is much smaller than the standard deviation found at comparing both codes (~20%).

We also present the comparison between our B/T ratio and GIM 2D in Fig. 4. The global properties of the galaxies r_e and B/T are shown to be very robust for this sample of galaxies. In the nearby Universe, Sien & de Vaucouleurs (1986), using a $n=4$ bulge, did an estimation of the B/T ratio for a sample of galaxies ranging a large variation of morphological types. Graham (2001) conducted a similar analysis using this time a n free bulge. He found that the use of a $n=4$ bulge (instead of a n free) produces an overestimation of the B/T ratio. We do not see a strong difference between our B/T values and the GIM 2D estimations. This is probably due to most of our galaxies having small B/T ratios and consequently the bulge component is not dominant. However, the use of a different model for the bulge will have consequences when dealing with bulge properties such as $r_{e,b}$.

We also compare our B/T determination with the morphological type obtained from van den Bergh et al. (1996, hereafter vdB 96). This is shown in Fig. 5. The numerical classification used by vdB 96 (Abraham et al. 1996) is as follows: E/star: -1, E: 0, E/S0/Sa: 1, S0/Sa: 2, Sa/Sab: 3, Sb/S/Irr: 4, Sc: 5, Ir: 6, Peculiar/Mergers: 7 or 8. As explained before, galaxies with $B/T > 0.6$ were reanalysed and

Table 4. Coarse comparison of galaxy classifications in the HDF (N down to $I_{814}(\text{AB}) < 24.5$ mag and $z < 1$ for the same group of galaxies using three different methods. The number of analysed galaxies is 102.

Type	B/T	This work	M S98	vdb 96
E/S0	> 0.5	20%	15%	22%
S/Irr	< 0.5	80%	85%	78%

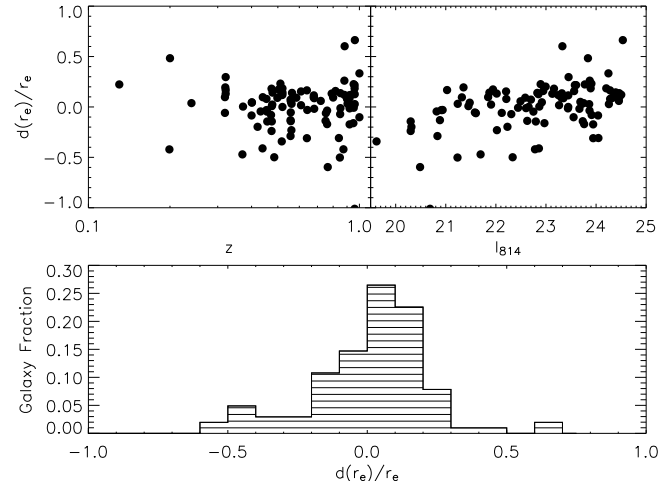


Figure 3. The relative error between the size estimation using our code and GIM 2D $d(r_e)/r_e = 2 \cdot (r_e(\text{GIM 2D}) - r_e(\text{ours})) / (r_e(\text{GIM 2D}) + r_e(\text{ours}))$ is shown versus z and versus the apparent I_{814} magnitude. The histogram shows that for 75% of the galaxies the difference on size is less than 20%.

tted with a bulge (only Sersic component (i.e. $B/T = 1$). For illustrative purpose, to avoid the appearance of just one point at $B/T = 1$ in Fig. 5, we have randomly moved all the galaxies with this B/T value a 5% around 0.95. The main difference between our analysis and M S98 is the group of galaxies classified by vdB 96 as $vdb = 0$. Contrary to M S98, most of the vdB 96 visual ellipticals are also classified as $B/T = 1$ in our quantitative analysis.

The fractions of the different morphological types according to vdB 96 (down to $I_{814}(\text{AB}) < 25$ mag and not z restrictions) are: 30% E/S0, 31% S/Irr and 39% not classified. However, these percentages depend on the limiting magnitude and the limiting redshift used. To make a reasonable comparison between the different morphological types which follow from the three different methods (ours, M S98 and vdB 96) we have used exactly the same galaxies. Our results are presented on Table 4. As we can see the agreement between the different methods is good. Consequently, previous claimed discrepancies between visually and quantitative methods (M S98) are shown here to be potentially due to different limiting magnitude criteria and redshift. However, although the fractions may be similar for each study, different galaxies may populate each bin. We have checked if this is the case by comparing galaxy by galaxy and found that the agreement in each bin is greater than 65%.

We have also undertaken a comparison with the analysis done in the HDF (S by Moth & Elston (2002)). In that work, 33 galaxies with $0.56 \leq z \leq 1.2$ and $I_{814} < 25$ are analysed. The model used for extracting structural information is a

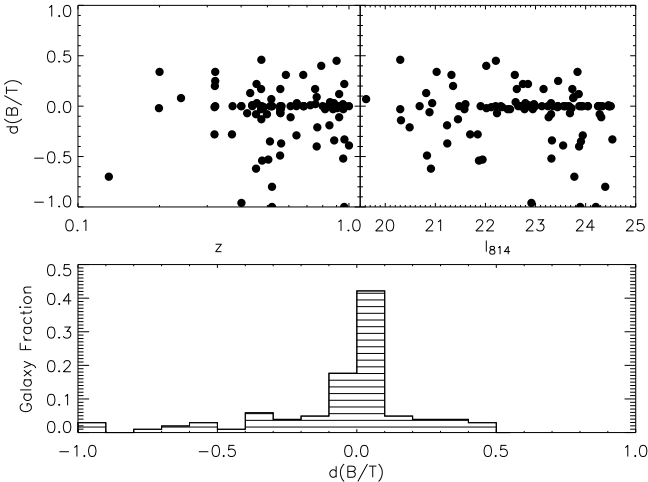


Figure 4. The difference between the B/T estimation using our code and GIM 2D $d(B/T) = B/T(GIM 2D) - B/T(\text{ours})$ is shown versus z and versus the apparent I_{814} magnitude. The histogram shows that for 73% of the galaxies B/T differs less than 0.2 units.

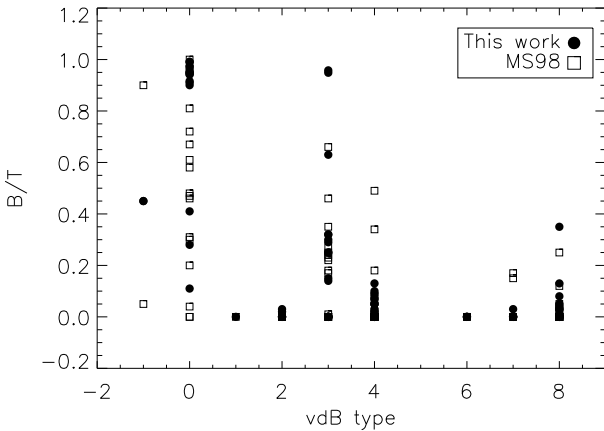


Figure 5. Comparison of the parameter B/T with the vdB morphological type derived from the visual classification of van den Bergh et al. (1996).

single Sersic law and not a bulge+disc decomposition. For that reason the comparison is not straightforward. For the 20 galaxies we have in common, we find a very good agreement in the global size (difference less than 20%) for 18 objects (90%). A similar analysis using also a single Sersic law is done in Trujillo et al. (2004) for K_s -band selected galaxies down to $K_s = 23.5$. Trujillo et al. analysed in the I_{814} band galaxies up to $z = 0.8$. The agreement in the global sizes for the common 61 galaxies is good, with 68% of the objects having a difference less than 10%.

6 COMPLETENESS AND REDSHIFT-DEPENDENT SELECTION EFFECTS

The ability to detect a galaxy is critically dependent on its apparent surface brightness. Galaxies with larger B/T are easier to detect because they are more concentrated, and galaxies with larger radii are harder to detect than smaller

ones at given total magnitude. Therefore, it is of interest to know whether our observed parameter distribution would be biased by the galaxy selection function of the SExtractor detection algorithm (used in both catalogs we are using). The evaluation of completeness of the HDF{N was carefully modelled in detail by MS98 (their Fig. 5). According to these authors galaxies brighter than $I_{814}(AB) < 24.5$ are fully recovered. Due to the very similar characteristics of the HDF{S these results are also valid for that field. This means that in the sample of galaxies shown in this work the incompleteness is not playing any role and consequently we will not take it into account in the subsequent analysis.

Redshift-dependent observational biases can also mimic real evolutionary changes in the galaxy population (Simard et al. 1999). For a given magnitude limit (in our case $I_{814}(AB) = 24.5$ mag) there is a corresponding threshold in the observable restframe luminosity which increases with redshift. We illustrate this in Fig. 6. This figure shows the restframe luminosity in the V-band versus the redshift.

To estimate the restframe luminosity in the V-band we make use of the complete filter coverage of the HDFS. We have used the fluxes measured in the $U_{300}, B_{450}, V_{606}, I_{814}, J, H$ and K bands provided by the Fernandez-Soto et al. (1999; HDF{N) and Labbe et al. (2003; HDF{S) catalogs. With these fluxes we construct observed SEDs for every galaxy. As we have redshift data for our sources we estimate the redshifted wavelength of the center of the local V-band filter ($\lambda = 5510 \text{ \AA}$) (i.e. we evaluate $\lambda = 5510(1+z)$). At that wavelength, we measure the restframe V-band flux by linearly interpolating the catalog's fluxes at the two closest values. The advantage of using this method is that we do not rely on any SED model to estimate the luminosity. There are two main sources of uncertainty:

(i) The uncertainty due to the photometric redshifts: most of our galaxies (70% in the HDF{N and 60% in the HDF{S) have z spectroscopically determined, however, the remaining fractions have an uncertainty of $dz/(1+z) = 0.1$. This uncertainty in z can be translated into luminosity uncertainty of 30%.

(ii) The uncertainty due to the total flux calibration: the reliability of the total flux measured through a given filter will depend on the S/N of the sources. Fortunately, the HDFS are so deep, and the objects selected in this work so bright, that this effect does not play a major role. In fact, we can see from the comparison between our magnitudes (which are an extrapolation of the total magnitude up to an infinite radial extension) and the aperture magnitude (our Fig. 2) that the mean discrepancies between both is 0.2 mag, being the "true" flux value probably in between these two estimates. The above uncertainty in the magnitude is translated into a luminosity uncertainty of 20%.

According to the above two points we will assume on what follows an uncertainty in the restframe V-band luminosities of 35%.

In Fig. 6 we show how our high- z sample represents only the most luminous fraction of the galaxy population. The lack of bright galaxies at low redshift results directly from their low volume densities coupled with the small volume of the HDFS over this redshift range. Galaxies with $L_V > 2 \times 10^9 h^{-2} L_\odot$ (i.e. $M_B < -17.5$ assuming $B-V=0.9$) can be studied along the full redshift range.

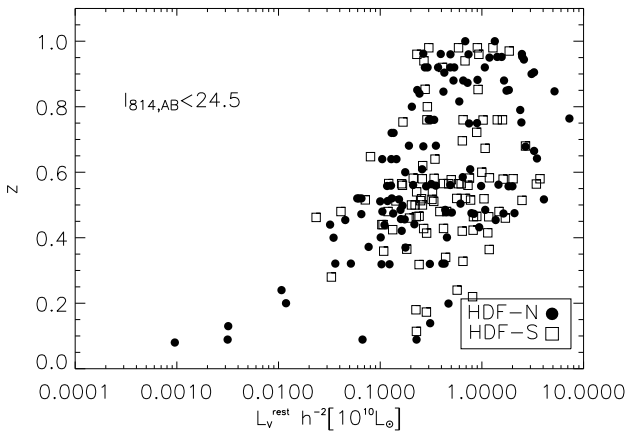


Figure 6. The L_v - z diagram for the objects selected in our sample with I_{814} (AB) < 24.5 mag.

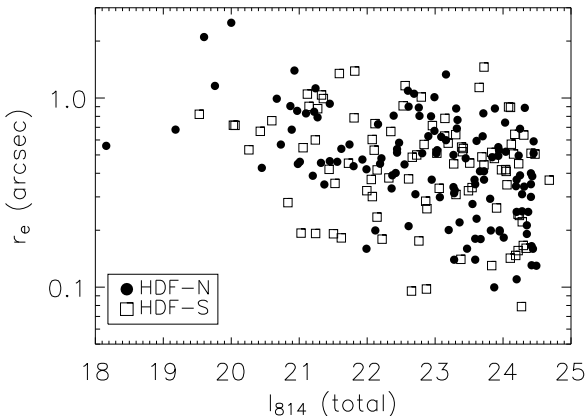


Figure 7. The relation between the model-independent global magnitude versus the apparent global semi-major effective radius size (in the I_{814} band).

7 H D F {N A N D H D F {S L U M I N O S I T Y {S I Z E R E L A T I O N S O U T T O Z = 1

It is of interest to know whether the population of galaxies in the H D F {N and H D F {S present similar global structural properties. We show in Fig. 7 the relation between the model-independent global magnitude versus the apparent global semi-major effective radius size (in the I_{814} band). We have run the generalization of the Kolmogorov-Smirnov (K-S) test on two dimensional distributions (Fasano & Franceschini 1987) and found that the null hypothesis (i.e. that the two distribution have a similar origin) can not be rejected.

In what follows, to facilitate the comparison with local calibrating data, we use, instead of the global semi-major effective radius r_p , the circularized effective radius $r_{e,c}$ (i.e. we use $r_{e,c} = r_e (1 - \epsilon)$ with the intrinsic, non-PSF affected, projected ellipticity of the galaxy). For those galaxies where $B/T < 1$, $\epsilon = d$. To be sure that the estimate of the intrinsic ellipticity of our sources, and hence the conversion to circularized effective radius, was not systematically affected by the PSF effect we studied the presence of any obvious

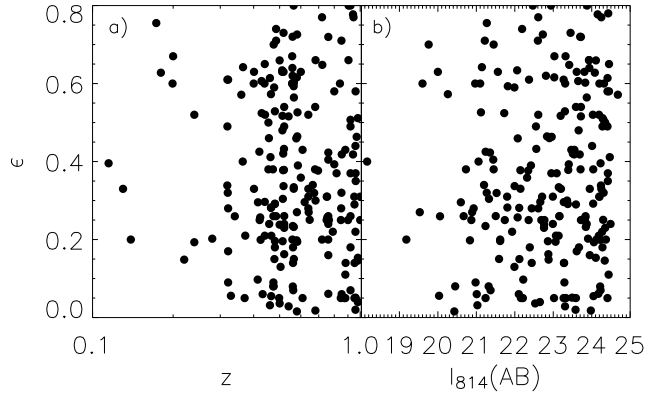


Figure 8. The intrinsic (i.e. the recovered non-PSF affected) ellipticity of the galaxies versus: a) the redshift of the observed sources and b) the apparent I_{814} total magnitude. No clear relation is observed.

trend with z or the I_{814} apparent magnitude (Fig. 8). No clear relation is found.

We have conducted a similar analysis to that presented in Fig. 7 using the rest-frame properties of the above galaxies. This is shown in Fig. 9a. In this case, the null hypothesis also can not be rejected. To avoid any bias due to K-S corrections we have used for galaxies with $z < 0.4$ the structural parameters obtained in the F606W filter (Table 2). For galaxies with $0.4 < z < 1$ the filter used was F814W. Therefore the sizes are computed for roughly the same rest-frame wavelengths (between B and V) over the entire redshift range. This avoids any band-dependent size effects. This would be particularly important in late-type galaxies. In the local universe, Graham (2001) finds (assuming that the effective radius of the bulge is not modified) that the scale of the discs increases 15-25% from R to B band.

In Fig. 9b we show the same sample but making a separation between early-type ($B/T > 0.5$) and late-type ($B/T < 0.5$) galaxies. At a fixed luminosity, late-type galaxies are larger than the early-types.

7.1 Testing the hypothesis of evolution

Shen et al. (2003) have shown the median and dispersion of the distribution of the circularized half-light radius (Banton et al. 2003) for different bands as a function of the luminosity in the Sloan Digital Sky Survey (SDSS, York et al. 2000). Their analysis is based on an unprecedented large database of nearby galaxies with typical $z = 0.1$. In the following, we closely match the analysis presented in Trujillo et al. (2004). We use the SDSS g-band (the closest available filter to our V-band) size distributions (S. Shen, 2003, private communication) as a local reference of the size distribution of galaxies in the nearby universe. The median and dispersion of the Shen et al. distribution in the g-band separating into early and late type are shown in Fig. 10. We also overplot our H D F s data.

The criteria followed to separate between early and late types in the presented SDSS relations is different from the one we have used. In the Shen et al. distributions a galaxy is separated into early or late type according to whether its

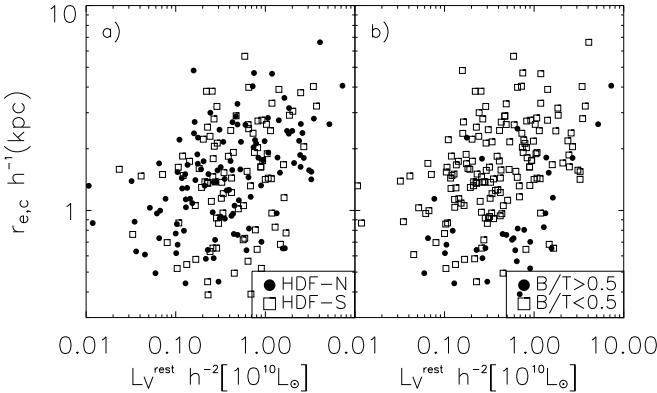


Figure 9. a) The distribution of circularized rest-frame sizes versus the rest-frame V-band luminosities is shown separating galaxies according to their ownership to the HDF{N or to the HDF{S. b) Same as a) but this time segregating the points between late-type ($B/T < 0.5$) and early-type ($B/T > 0.5$) galaxies. For clarity error bars are not shown. The mean size relative error is 20% and the mean luminosity error 30%.

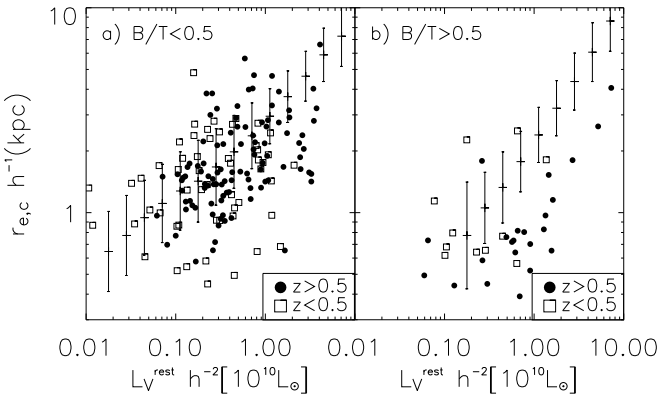


Figure 10. a) The distribution of rest-frame sizes versus the rest-frame V-band luminosities is shown for late-type ($B/T < 0.5$) galaxies. b) Same as a) with early-type ($B/T > 0.5$) galaxies. The points are separated according to the z value. For clarity error bars are not shown. The mean size relative error is 20% and the mean luminosity error 30%.

global Sersic index n is larger or smaller than 2.5. The index n derived for these authors corresponds to a global Sersic fit to the whole galaxy, whereas we have used a bulge+disc decomposition and our index n refers only to the bulge component. The separation between early and late type according to the global index n can be affected by the inclusion of some Sa galaxies as early-type galaxies. This effect is well illustrated by Ravindranath et al. (2004, their Fig. 1). Also, some contamination in the late-type galaxies at lower luminosities is expected from dwarf ellipticals which have $n < 1$.

7.1.1 Late-Type galaxies

At a given luminosity, Shen et al. propose for nearby galaxies the following size log-normal distribution with median r_e and logarithmic dispersion :

$$f(r_e | r_e(L), (L)) = \frac{1}{2} \frac{\ln^2(r_e - r_e(L))}{(L)} e^{-\frac{\ln^2(r_e - r_e(L))}{2(L)}} \frac{dr_e}{r_e}; \quad (6)$$

To address the problem of size evolution, we have assumed that the functional form of the size log-normal distribution function (Eq. 6) found for nearby galaxies also holds at all redshifts, but with evolving parameters:

$$r_e(L; z) = r_e(L; 0)(1 + z) \quad (7)$$

$$(L; z) = (L; 0)(1 + z) \quad (8)$$

Here, $r_e(L; 0)$ and $(L; 0)$ are the median size and dispersion provided at $z=0$ by the Shen et al. (2003) data, and r_e and (L) describe the redshift evolution. Implicit in Eq. 7 and Eq. 8 we assume the same size evolution for all the galaxies independently of their luminosity. However, in order to assure that we observe the same type of galaxies along the explored redshift range $0 < z < 1$ (see Fig. 6) we select only galaxies with $L_v > 2 \cdot 10^9 h^{-2} L_\odot$. To explore in much detail the evolution of the luminosity-size relation with z we have separated our sample in galaxies with $z < 0.5$ (mean $z = 0.4$) and galaxies with $z > 0.5$ (mean $z = 0.7$). The number of galaxies with $L_v > 2 \cdot 10^9 h^{-2} L_\odot$ is 31 in the lower z bin and 85 in the higher. Due to the scarce number of objects in the lower z bin we will concentrate our analysis on the galaxies with $z > 0.5$. In addition, there is a group of outliers with $z < 0.5$, luminosities between $0.1 \cdot 10^{10} h^{-2} L_\odot$ and small sizes that affects our analysis at lower redshifts. These galaxies have all spectroscopically determined for this bin is not useful because of the few number of galaxies then available.

We evaluate and using a Maximum Likelihood Method. The likelihood to maximize is given by:

$$L = \prod_{i=1}^n f(g_L g_{r_e}) \quad (9)$$

Each member (one per galaxy measured) of the product is a convolution between the expression f given in Eq. 6 and a gaussian representing the error on the luminosity g_L and another gaussian representing the error on the size g_{r_e} . The width of each gaussian is given by the error at estimating the luminosity and the size respectively.

The result of this analysis is shown in Fig. 11. According to this analysis the luminosity-size distribution of disc galaxies presents a slightly (although compatible with zero) broader dispersion at higher redshift. The dispersion increases by 20 (25)% . To know whether this increase in the dispersion is real or not will require a large number of galaxies.

We observe a moderate decrease in the sizes 30 (10)% at $z > 0.5$. In the luminosity-size distribution a decrease in the size can also be interpreted as an increase in the luminosity of the objects. In fact, this seems to be a plausible hypothesis to explain the observed luminosity-size evolution found at high z . According to the studies of the evolution of the stellar mass-to-light ratio (see e.g. Rudnick

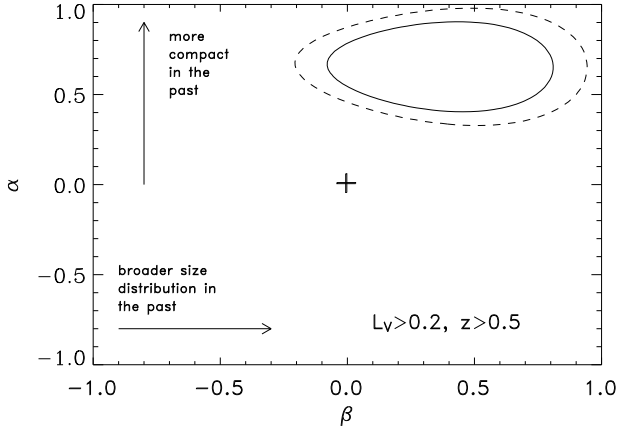


Figure 11. Luminosity-size evolution for late-type galaxies with $z > 0.5$. Likelihood contours representing the evolution in size and dispersion in the $\{$ plane. Solid line represents the 1 confidence level contour, dashed line the 2 confidence level. The cross shows the position of no evolution in this plane. Positive values of α represent decreasing values of the size with redshift. Positive values of β represent increasing the intrinsic dispersion of the population with redshift. The luminosities are given in $10^{10} L_\odot$.

et al. 2003) the stellar populations were younger at high $\{z\}$, and for that reason, the mass-to-light ratio is a decreasing function with z . Consequently, even though the size of the galaxies does not decrease with z , the luminosity evolution of the objects will simulate this effect. Consequently, our observed evolution in the luminosity-size distribution can be alternatively interpreted as a decrease in the central surface brightness of 0.77(0.30) mag at $z = 0.7$.

The results presented here are in agreement with those found by Lilly et al. (1998), Simard et al. (1999) and Ravindranath et al. (2004). These authors do not find a great change from local galaxies out to $z = 0.7$ and a hint of change at $z > 0.7$ with shorter objects than those locally observed for a similar magnitude range.

7.1.2 Early-type galaxies

In addition to the SDSS distribution and for covering the range of faint galaxies in the relation shown in Fig. 10b, we have used a local sample of 200 elliptical galaxies from the Virgo, Fornax and Coma cluster (Cao et al. 1990; 1994; Binggeli & Jerjen 1998; Gutierrez et al. 2004). This sample ranges from $-22 < M_B < -12$. To transform to V-band magnitudes we have used $B - V = 0.9$. To facilitate the comparison with this data, this time we use the semi-major effective radius. The result of this comparison is shown in Fig. 12.

It is interesting to note that the observed distribution, with a plateau at the faintest galaxies, is in qualitative good agreement with the distribution of galaxies found in nearby samples. The apparent absence of evolution in the shape of the distribution of galaxies in the size-luminosity relation suggests that the early-type galaxies were yet assembled at higher redshift (Fasano et al. 1998, van Dokkum & Ellis 2003, Franx et al. 2003, van Dokkum et al. 2003, Deaddie et al. 2003, Vazdekis, Trujillo & Yamaoka 2004). However, we observe that at a given size, high- z early-type galaxies present

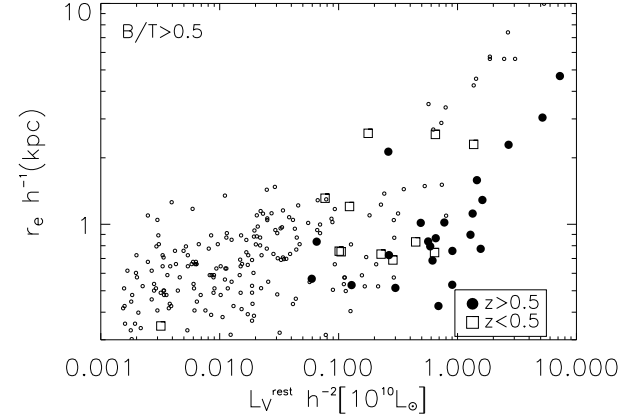


Figure 12. The distribution of rest-frame sizes versus the rest-frame V-band luminosities is shown for early-type ($B/T > 0.5$) galaxies. The points are separated according to the z value. Small open points correspond to 200 ellipticals from a nearby sample of Virgo, Fornax and Coma clusters. For clarity error bars are not shown. The mean size relative error is 20% and the mean luminosity error 30%.

higher luminosities than the local sample. To quantify this increase we have fitted the early-type luminosity-size relation of the SDSS by using an expression of the form:

$$r_e = a L_V^b \quad (10)$$

We find the following values: $a_{SDSS} = 2.25$ and $b_{SDSS} = 0.65$. We have repeated the same exercise this time in our $z > 0.5$ early-type sample. Due to the scarcity of points we have fixed the b slope to the same value than the SDSS sample. To make the fit we use the points defined by the giant ellipticals (i.e. those points with $L_V > 10^{10} h^{-2} L_\odot$). On doing that we find: $a_{HDFs} = 1.05$. This implies a factor of 3.5(0.25) greater in luminosity which corresponds to 1.35(0.10) mag. This is in good agreement with the brightening of 1.15 mag observed in the rest-frame B-band by Im et al. (1996; 2002) and Schade et al. (1999) using the HST Medium Deep Survey and other HST fields. It is of interest to note that the comparison between SDSS and the HDFs are between field early-type galaxies. The bright elliptical galaxies in the nearby clusters define a relation with $a_{clusters} = 3.45$. Consequently, we find that early-type galaxies in the HDFs at $z = 0.7$ are a factor of 6.7 brighter in luminosity (2 mag) than the present-day elliptical in clusters. In agreement with previous studies that indicate that early-types in clusters are older than in the field.

We have checked, using a 2D KS test whether the no-evolution (versus the passive evolution) model can be ruled out. To do that we have used only the galaxies with $L_V > 0.1 \cdot 10^{10} h^{-2} L_\odot$ and $z > 0.5$. This test rejects the no-evolution hypothesis with a confidence larger than than 99.9%. This luminosity evolution is consistent with models in which the bulk of stars in the field E/S0 galaxies formed before $z > 1.5$ and have been evolving rather quiescently.

8 DISCUSSION AND CONCLUSIONS

It is of interest to compare the results presented in this paper with the theoretical expectations according to the different scenarios of galaxy formation.

In the hierarchical scenario, following Mo et al. (1998), the size of the baryonic component of disc galaxies is expected to scale with redshift as $R / H^{-1}(z)$ at fixed circular velocity, or $R / H^{2/3}(z)$ at fixed mass. In a flat universe $\Omega = 1$, the Hubble constant evolves with redshift as:

$$H(z) = H_0 [1 + \Omega_0 (1 + z)^3]^{1/2} \quad (11)$$

where Ω_0 and Ω are the present-day density parameters. At $z = 0.7$ (the mean z of our high- z population), the expected evolution is $0.68 < R(0.7)/R(0) < 0.77$. This decrease is compatible with our estimation: $30 \pm 10\%$. However, before extracting any conclusion we must take into account that the Mo et al. predictions are for the mass-size relation whereas this work deals with the luminosity-size relation. In fact, according to previous (Trujillo et al. 2004) and ongoing (Barden et al. 2004; private communication) work, although the luminosity-size relation has changed dramatically from $z = 3$, the stellar mass-size relation has remained nearly invariant from then.

In the infall scenario, for the rest-frame B-band, Bouwens & Silk (2002) propose the following dependence in size: $R(z)/R(0) = 1 - 0.27z$. At $z = 0.7$ this corresponds to a decrease of 19%. This value is in agreement (although is slightly smaller than the observed) with our measurements. Contrary to the above predictions of the hierarchical models, the Bouwens & Silk prediction is for the luminosity-size relation, and consequently, the comparison with our observations is a more direct one. It is important to note, however, that our analysis is done in the V-band, and the expected evolution from the Bouwens & Silk (2002) model could be slightly different in this band.

As pointed out by Bouwens & Silk (2002): 'The hierarchical and infall models predict relatively similar amounts of evolution in global properties (size, surface brightness, and luminosity) for disc galaxies to $z = 1$ '. This implies we need to find an extra test for disentangle between both scenarios. The main difference between both approaches is the evolution of the comoving number density of the objects. In the infall models is implicitly assumed no number evolution whereas in the hierarchical model the number of disc galaxies, is an increasing function of z : $N(V_c, z)dV_c / (1 + z)^{(2.9 - 3.3)}$ at a fixed circular velocity, or $N(L, z)dL / (1 + z)^{(1.45 - 1.85)}$, at a fixed luminosity (see e.g. Mao, Mo & White 1998). The scarce number of galaxies in this work and the strong field-to-field variations prevent a definitive answer at this point and larger areas are required.

Contrary to the disc galaxies, the number of E/S0s decreases at high- z in the hierarchical picture. However, in a flat non-zero universe the semi-analytical models predict a weak number density evolution. This makes difficult to disentangle between the monolithic evolution scenario and the hierarchical view up to $z = 1$. A more definitive answer to this problem will come from studying in detail the population of E/S0s galaxies in the $1 < z < 2$ interval.

ACKNOWLEDGMENTS

We are happy to thank Shiyin Shen for providing us with the Sloan Digital Sky Survey data used in this paper. We are grateful to Marco Barden, Eric Bell, Ivo Labbe, Daniel H. M. McIntosh, Hans Walterrix and Gregory Rudnick for interest and useful discussion. We also would like to thank David Butler for kindly proofreading parts of this paper. We wish to thank the anonymous referee for the helpful comments.

Based on observations made with the NASA/ESA Hubble Space Telescope, obtained from the data archive at the Space Telescope Institute. STScI is operated by the association of Universities for Research in Astronomy, Inc. under the NASA contract NAS 5-26555.

Funding for the creation and distribution of the SDSS Archive has been provided by the Alfred P. Sloan Foundation, the Participating Institutions, the National Aeronautics and Space Administration, the National Science Foundation, the US Department of Energy, the Japanese Monbukagakusho, and the Max-Planck Society. The SDSS Web site is <http://www.sdss.org>. The SDSS is managed by the Astrophysical Research Consortium (ARC) for the Participating Institutions. The Participating Institutions are the University of Chicago, Fermilab, the Institute for Advanced Study, the Japan Participation Group, Johns Hopkins University, Los Alamos National Laboratory, the Max-Planck-Institut für Astronomie (MPIA), the Max-Planck-Institut für Astrophysik (MPA), New Mexico State University, University of Pittsburgh, Princeton University, the US Naval Observatory, and the University of Washington.

REFERENCES

- Abraham, R.G., van den Bergh, S., Gazebo, K., Ellis, R.S., Santiago, B.X., Surma, P., Griffiths, R.E., 1996, ApJS, 107, 1
- Abramowitz, M., Stegun, I., 1964, Handbook of Mathematical Functions, Dover, New York.
- Aguerri, J.A.L. & Trujillo, I., 2002, MNRAS, 333, 633
- Aguerri, J.A.L., Iglesias-Páramo, J., Vázquez, J.M. & Muñoz-Tunón, C., 2004, AJ, 127, 1344
- Aguerri, J.A.L. & Trujillo, I., 2004, in preparation (Paper II)
- Andredakis, Y.C., Peletier, R., Balcells, M., 1995, MNRAS, 275, 874
- Banton, M.R., et al., 2003, ApJ, 592, 819
- Barden, M., et al., 2004, in preparation
- Bell, E.F., Wolf, C., Meisenheimer, K., Rix, H.-W., Borch, A., Dye, S., Kleinheinrich, M., McIntosh, D.H., 2004, ApJ, submitted, astro-ph/0303394
- Binggeli, B., & Jerjen, H., 1998, A&A, 333, 17
- Bouwens, R.J., Cayon, L., & Silk, J., 1997, ApJ, 489, L21
- Bouwens, R.J., & Silk, J., 2002, ApJ, 568, 522
- Cao, N., Capaccioli, M., & Ramírez, R., 1990, A&AS, 86, 429
- Cao, N., Capaccioli, M., & D'Onofrio, M., 1994, A&AS, 106, 199
- Cayon, L., Silk, J., & Charlot, S., 1996, 467, L53
- Casertano, S., et al., 2000, AJ, 120, 2747
- Chiosi, C., & Carraro, G., 2002, MNRAS, 335, 335

- Coleman G. D., Wu C.-C., Woodward D. W., 1980, *ApJS*, 43, 393
- Daadi E. et al. 2003, *ApJ*, 588, 50
- Eggen O. J., Lynden-Bell D. & Sandage, A. R., 1962, *ApJ*, 136, 748
- Fasano G. & Franceschini A., 1987, *MNRAS*, 225, 155
- Fasano G., Cristianini S., Amoutsos S. & Filippi M., 1998, *AJ*, 115, 1400
- Fernandez-Soto A., Lanzetta K. M., & Yahil A., 1999, *ApJ*, 513, 34
- Franx M. et al. 2003, *ApJ*, 587, L79
- Freeman K., 1970, *ApJ*, 160, 811
- Graham A. W., 2001, *AJ*, 121, 820
- Graham A. W. et al. 2004, in preparation
- Gutierrez C. M., Trujillo I., Aguerri J. A. L., Graham A. W., Caon N., 2004, *ApJ*, 602, 664
- Im M., Griffiths, R. E., Ratnatunga, K. J., & Sarajedini V. L., 1996, *ApJ*, 461, L79
- Im M. et al., 2002, *ApJ*, 571, 136
- Kaumann G., Colberg J. M., Diaferio, A., & White, S. D. M., 1999, *MNRAS*, 307, 529
- Kaumann G. & Charlton, S., 1998, *MNRAS*, 297, 23
- Labbe I. et al. 2003, *AJ*, 125, 1107
- Larson R., 1975, *MNRAS*, 173, 671
- Lilly S. et al. 1998, *ApJ*, 500, 75
- Mao S., Mo H. J., & White S. D. M., 1998, *MNRAS*, 297, L71
- Marleau F. R., & Simard L., 1998, *ApJ*, 507, 585 (M98)
- Mo H. J., Mao S. & White S. D. M., 1998, *MNRAS*, 295, 319
- Mooth P. & Elston R. J., 2002, *AJ*, 124, 1886
- Peng C. Y., Ho L. C., Impey C. D. & Rix H. W., 2002, *AJ*, 124, 266
- Press W. H., Teukolsky S. A., Vetterling W. T. & Flannery, B. P. 1992, *Numerical Recipes* (Cambridge: Cambridge Univ. Press)
- Ravindranath, S. et al. 2004, *ApJ*, 604, L9
- Roche N., Ratnatunga K., Griffiths R. E., Im M., Naim A., 1998, *MNRAS*, 293, 157
- Rudnick G. et al. 2001, *AJ*, 122, 2205
- Schade D., Lilly S. J., Crampton D., Hammer F., Le Fevre O., & Tresse L., 1995, *ApJ*, 451, L1
- Schade D., Lilly S. J., Le Fevre O., Hammer F., Crampton D., 1996, *ApJ*, 464, 79
- Schade D. et al. 1999, *ApJ*, 525, 31
- Sersic J., 1968, *Atlas de Galaxias Australes* Cordoba: Observatorio Astronomico
- Shen S., Mo H. J., White S. D. M., Blanton M. R., Kaumann G., Voges W., Brinkmann J., Csabai I., 2003, *MNRAS*, 343, 978
- Simard L. 1998, in ASP Conf. Ser. 145, *Astronomical Data Analysis Software System* V II, ed. R. A. Ibáñez, R. N. Hook, & H. A. Bushouse (San Francisco: ASP), 108
- Simard L. et al. 1999, *ApJ*, 519, 563
- Simien F. & de Vaucouleurs, G., 1986, *ApJ*, 302, 564
- Somerville R. S. & Primack, J. R., 1999, *MNRAS*, 310, 1087
- Toomre A., & Toomre J., 1972, *ApJ*, 178, 623
- Trujillo I., Aguerri, J. A. L., Gutierrez C. M., & Cepa J., 2001a, *AJ*, 122, 38
- Trujillo I., Aguerri J. A. L., Cepa J. & Gutierrez, C. M., 2001b, *MNRAS*, 328, 977
- Trujillo I., Aguerri J. A. L., Cepa J. & Gutierrez, C. M., 2001c, *MNRAS*, 321, 269
- Trujillo I., Graham A. W., Caon N., 2001, *MNRAS*, 326, 869
- Trujillo I., et al. 2004, *ApJ*, 604, 521
- van den Bergh S., Abraham R. G., Ellis, R. S., Tanvir N. R., Santiago, B. X. & Gazebo, K. G., 1996, *AJ*, 112, 359 (vdB 96)
- van Dokkum P. G. & Ellis R. S., 2003, *ApJ*, 592, L53
- van Dokkum P. G. et al. 2003, *ApJ*, 587, L83
- Vazdekis A., Trujillo I., & Yamada, Y., 2004, *ApJ*, 601, 33L
- White S. D. M. & Frenk, C. S., 1991, *ApJ*, 379, 52
- Williams R. E. et al., 1996, *ApJ*, 112, 1335
- York D. et al., 2000, *AJ*, 120, 1579